Unified microscopic approach to the description of elastic and inelastic cross sections of reactions with heavy ions

K. V. Shitikova

Scientific-Research Institute of Nuclear Physics, Moscow State University
Fiz. Elem. Chastits At. Yadra **16**, 824–874 (July–August 1985)

A microscopic approach to the study of the elastic and inelastic cross sections of reactions with heavy ions that has as its aim the investigation of possible manifestations of nuclear structure in these processes is presented. The interaction potential of heavy nuclear particles is constructed with inclusion in the computational scheme of the numerical values for the nuclear densities as obtained in microscopic approaches—in the method of hyperspherical functions for light ions and the quasiparticle—phonon model for heavy ions. The reactions in which the ions ^{4}He, ^{6}Li, ^{12}C, ^{16}O are scattered by one another and also by the targets ^{58,60}Ni, ^{90}Zr, ^{124}Sn, ^{142,144}Nd, ^{208}Pb are studied.

INTRODUCTION

In the present review, a unified microscopic approach to the description of elastic and inelastic cross sections of reactions with heavy ions is proposed and developed.

The interaction potential of heavy nuclear particles has been constructed with inclusion in the computational scheme of the numerical values for the nuclear densities as obtained in the framework of the microscopic approach and tested on experimental data. A unified description of elastic and inelastic reaction cross sections has been made possible by the construction of the heavy-ion interaction matrix elements—the diagonal elements for the ground and excited states, and also nondiagonal matrix elements. The heavy-ion scattering cross sections have been calculated with one free parameter, only the amplitude of the forces in the imaginary part of the optical potential having been varied.

This approach was proposed for the first time in Refs. 1 and 2 and was used there to investigate elastic and inelastic cross sections for ions with $A \leqslant 16$. The nuclear-matter density distributions obtained in the method of hyperspherical functions[3–5,11] were included in the computational scheme. The possible manifestations of giant monopole resonances of light nuclei in reactions with heavy ions were studied[2] in this formalism. These investigations are topical, on the one hand, because the experimental detection of giant monopole resonances in light nuclei ($A \leqslant 16$) is still the subject of debate. On the other hand, the method of hyperspherical functions is supposed to make reliable theoretical predictions in the description of monopole vibrations and can be applied to the study of inelastic processes in reactions with ions in which monopole degrees of freedom are excited. A necessary intermediate stage here is the detailed investigation of the possibilities of the method for describing elastic scattering of ions. For this reason, the elastic cross sections were studied in the proposed method in Refs. 6–9.

In fact, in Ref. 6 it was shown that the experimental data on elastic scattering of heavy ions at different energies can be reproduced only if the amplitude of the imaginary part of the optical potential is reduced.

In Ref. 7, analytic double-folding potentials with finite-range forces of Gaussian type as proposed by Satchler and Love were obtained. They were used to construct various folding potentials for combinations with $A = 4, 6, 12, 16$ and to calculate the ^{4}He–^{12}C elastic cross section. A theoretical investigation of ^{16}O–^{16}O elastic scattering at various energies of the incident ions was also made.[8] The nuclear interaction potentials of heavy ions were constructed in the folding model with both δ-function and finite-range forces, and also in the energy-density formalism. Finally, in Ref. 9 the field of application of the proposed approach was extended to heavier ions, and the elastic scattering of ^{6}Li, ^{12}C, ^{16}O on the nuclei ^{58,60}Ni, ^{90}Zr, ^{124}Sn, ^{142,144}Nd, ^{208}Pb was studied. For the light ions, the densities obtained by the method of hyperspherical functions were used in this case. The nuclear densities for the heavy ions were obtained in the framework of the quasiparticle-phonon model.[10] The interaction potential of the heavy nuclear particles was constructed in the folding model with an effective nucleon–nucleon (NN) interaction of the Yukawa type M3Y. The investigation showed that overall it is possible to reproduce the experimental results with just one free parameter. The microscopic structure of the wave functions of the investigated nuclei is manifested in these calculations. The amplitude of the imaginary part of the optical potential has less influence in the case of the heavy ions on the results of the calculation of the elastic-scattering cross sections than it does for light ions.

The main aim of this review is to present the microscopic approach to the description of elastic and inelastic cross sections of reactions with heavy ions, showing how one can study the manifestation of nuclear structure in these processes. Section 1 gives the method of theoretical description of the elastic and inelastic cross sections of reactions with heavy ions. It is shown how one can find the microscopic nuclear density and construct the nuclear potential of heavy ions in the folding model and in the energy-density formalism; a method for calculating the angular distributions of the elastic and inelastic cross sections is explained.

Section 2 presents the results of calculations and com-

 0090-4759/85/040364-25$04.40

pares them with experimental data on the cross sections of elastic heavy-ion reactions and inelastic reactions in which the monopole resonance is excited.

1. METHOD OF CALCULATION

In this section, a method for calculating elastic and inelastic cross sections of reactions with heavy ions is presented. The interaction potential of heavy nuclear particles has been constructed in the folding model or in the energy-density formalism, the densities obtained in the framework of microscopic models being used for its construction. Thus, the densities for light nuclei were calculated in the method of hyperspherical functions. The nuclear densities for heavy ions were found in the framework of the quasiparticle-phonon model. Knowledge of the nature of the wave function that participates in the calculations opens up the possibility of investigating nuclear structure in heavy-ion reactions. The nuclear interaction potentials obtained for the heavy ions in the ground and excited states were then included in the scheme for calculating the elastic and inelastic reaction cross sections. It was assumed that the imaginary potential must have the same form as the real potential. Therefore, the cross sections were calculated using just one free parameter. This parameter was normalized in the elastic channel.

Nuclear densities in the method of hyperspherical functions[3,4,11]

We begin with a brief exposition of the method of obtaining the densities of light nuclei in the method of hyperspherical functions.[3,4,11] These densities will then be used to describe the light ions.

The essence of the method of hyperspherical functions consists of the introduction of a convenient orthonormal system of many-particle functions, i.e., a hyperspherical basis, and in the creation of a mathematical formalism for working with them. In this method, there is no need to introduce into the calculations any external parameters apart from the form and structure of the *NN* potentials; real *NN* interactions are used.

A specific feature of the method of hyperspherical functions (or the method of K harmonics) is that spherical coordinates are introduced in the $3(A-1)$-dimensional space of Jacobi coordinates: the hyperradius ρ and hyperspherical angles (in number, $3A-4$); and the nuclear wave function Ψ is expanded with respect to standard functions of these angles-hyperspherical harmonics.

The hyperspherical angles $\theta_1, \theta_2, \ldots, \theta_{n-1}$ can be chosen in such a way that the relationship between the Cartesian and hyperspherical coordinates has the form

$$\left.\begin{aligned} &x_1 = \rho \sin\Theta_{n-1} \ldots \sin\Theta_2 \sin\Theta_1;\\ &x_2 = \rho \sin\Theta_{n-1} \ldots \sin\Theta_2 \cos\Theta_1;\\ &\ldots\ldots\ldots\ldots\ldots\ldots\\ &x_{n-1} = \rho \sin\Theta_{n-1} \cos\Theta_{n-2};\\ &x_n = \rho \cos\Theta_{n-1};\\ &\rho^2 = \sum_{i=1}^{n} x_i^2, \quad 0 \leqslant \rho \leqslant \infty,\\ &\qquad\qquad 0 \leqslant \Theta_i < 2\pi. \end{aligned}\right\} \tag{1}$$

The volume element dV in the n-dimensional space is written in the form

$$dV = dx_1 dx_2 \ldots dx_n = \rho^{n-1} d\rho\, d\Omega, \tag{2}$$

with the element of solid angle

$$d\Omega = \sin^{n-2}\Theta_{n-1} \sin^{n-3}\Theta_{n-2} \ldots \sin\Theta_2\, d\Theta_{n-2} d\Theta_{n-2} \ldots d\Theta_1. \tag{3}$$

The Laplacian is given by

$$\Delta_n = \frac{1}{\rho^{n-1}} \frac{\partial}{\partial\rho}\left(\rho^{n-1}\frac{\partial}{\partial\rho}\right) + \frac{1}{\rho^2}\Delta_{\Omega_n}, \tag{4}$$

and the angular part of the n-dimensional Laplacian satisfies the recursion relation

$$\Delta_{\Omega_n} = \frac{1}{\sin^{n-2}\Theta_{n-1}} \frac{\partial}{\partial\Theta_n}\left(\sin^{n-2}\Theta_{n-1}\frac{\partial}{\partial\Theta_{n-1}}\right) + \frac{1}{\sin^2\Theta_{n-1}}\Delta_{\Omega_{n-1}}. \tag{5}$$

The hyperspherical harmonics are eigenfunctions of the angular part of the Laplacian,

$$\Delta_{\Omega_n} V_{K\nu}(\Theta_i) = -K(K+n-2)\, V_{K\nu}(\Theta_i), \tag{6}$$

where K is the analog of angular momentum in the case $n = 3$ and is called the global moment. The index ν includes all quantum numbers needed to designate the various degenerate states in Eq. (6). For ν, one usually employs the Young diagram $[f]$ and the Yamanouchi symbol (r), which characterize the properties of the K harmonics with respect to permutations of the A nucleons, and also L and M, the orbital angular momentum of the state and its projection.

Thus, in the method of hyperspherical functions the wave function of the A nucleus is represented as an expansion in the K harmonics $|AK[f]\varepsilon LST\rangle$:

$$\Psi = \sum_{K \geqslant K_{min}} \varphi_K^{K[f]\varepsilon LST}(\rho)\, |AK[f]\varepsilon LST\rangle, \tag{7}$$

where

$$\int \varphi_K^2(\rho)\, \rho^{3A-4} d\rho = 1. \tag{8}$$

The Hamiltonian of the nucleus has the form

$$H = -\frac{\hbar^2}{2m}\frac{1}{\rho^{3A-4}}\frac{\partial}{\partial\rho}\left(\rho^{3A-4}\frac{\partial}{\partial\rho}\right) - \frac{\hbar^2}{2m\rho^2}\Delta_\Theta + V. \tag{9}$$

If we substitute the function (6) in the Schrödinger equation and multiply the result by $\langle AK[f]\varepsilon LST|$, then we obtain a system of equations of the form

$$\left\{-\frac{\hbar^2}{2m}\frac{d^2}{d\rho^2} + \frac{\hbar^2 L_k(L_k+1)}{2m\rho^2} - E\right\}\chi_k^{k\varepsilon[f]LST}(\rho) + \sum_{\bar{k}\bar{\varepsilon}\bar{L}\bar{S}\bar{T}} W_{k\varepsilon LST[f]}^{\bar{k}\bar{\varepsilon}\bar{L}\bar{S}\bar{T}[\bar{f}]}(\rho)\, \chi_{\bar{k}[\bar{f}]\bar{\varepsilon}\bar{L}\bar{S}\bar{T}}(\rho) = 0. \tag{10}$$

Here, $L_k = K + (3A-6)/2$, $\chi_k = \rho^{(3A-4)/2}\varphi_k(\rho)$; the number of equations in this system and the number of terms in the sum (10) is equal to the number of terms included in the expansion (7). Attention should be drawn to the exceptionally strong centrifugal potential $L_k(L_k+1)/\rho^2$ in these equations; it is a consequence of the Pauli principle. The high values of L_k are due to the fact that the values of K_{min} compatible with the Pauli principle are large. The potentials

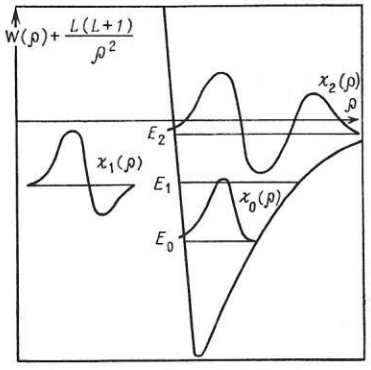

FIG. 1. Matrix element of effective interaction with inclusion of the centrifugal term in the method of hyperspherical functions and solutions in it: E_0, E_1, E_2; $\chi_0(\rho), \chi_1(\rho), \chi_2(\rho)$.

$W_k^{\bar{k}}(\rho)$ are matrix elements of the form

$$\langle AK[f]\varepsilon LSTM_LM_SM_T \mid \hat{V} \mid A\bar{K}[\bar{f}]\bar{\varepsilon}\bar{L}\bar{S}\bar{T}\bar{M}_L\bar{M}_S\bar{M}_T\rangle$$

$$= \frac{A(A-1)}{2}\langle AK[f]\varepsilon LST \mid V(r_{A-1,A}) \mid A\bar{K}[\bar{f}]\bar{\varepsilon}\bar{L}\bar{S}\bar{T}\rangle$$

$$= \frac{A(A-1)}{2} \sum_{K_2[f_2]\varepsilon_2L_2S_2T_2L_0S_0T_0\Lambda L'K'} \langle S_0T_0 \mid W_{\sigma\tau} \mid S_0T_0\rangle$$

$$\times R_{k'L_0}^{k\bar{k}}(\rho)\langle AK[f]\varepsilon LST \mid A-2K_2[f_2]\varepsilon_2L_2S_2T_2,\ \Lambda(L'K');$$

$$L_0S_0T_0\rangle$$

$$\times\langle A\bar{K}[f]\bar{\varepsilon}\bar{L}\bar{S}\bar{T} \mid A-2K_2[f_2]\varepsilon_2L_2S_2T_2,\ \Lambda(L'K');$$

$$L_0S_0T_0\rangle. \qquad (11)$$

Here

$$R_{K'L_0}^{K\bar{K}}(\rho) = \int d\Theta_1(\sin\Theta_1)^{3A-7}(\cos\Theta_1)^2 f(\rho\cos\Theta_1)$$

$$\times Q_{KK'L_0}^{A}Q_{\bar{K}K'L_0}^{A}(\sin\Theta_1)^{2K'}(\cos\Theta_1)^{2L_0}$$

$$\times P_{K-K'-L_0}^{K'+\frac{3A-6}{2}-1,\ L_0+\frac{1}{2}}(\cos 2\Theta_1)\,P_{\bar{K}-K'-L_0}^{K'+\frac{3A-16}{2}-1,\ L_0+\frac{1}{2}}(\cos 2\Theta_1). \qquad (12)$$

In Eq. (11), $\langle S_0T_0|W_{\sigma\tau}|S_0T_0\rangle$ is the spin-isospin part of the matrix element.

The basis of the method of hyperspherical functions is extremely convenient for the microscopic description of monopole vibrations; for it contains a collective variable (the hyperradius ρ) associated with the mean-square radius $\rho^2 = A\langle\bar{r}^2\rangle$ of the nucleus, i.e., it is related to the mean nuclear density. The excitations with respect to this variable correspond to monopole vibrations of the nucleus as a whole, and the density is a dynamical variable. Figure 1 shows the matrix element of the effective interaction $W(\rho)$ with inclusion of the centrifugal term. The solution of the system of differential equations (10) makes it possible to find its eigenvalues E_0, E_1, E_2 and radial eigenfunctions; the first solution corresponds to the ground state of the nucleus, and the following solutions correspond to the first, second, etc., monopole excitations.

By means of the radial functions $\chi(\rho)$ one can find the nuclear densities in the method of hyperspherical functions. Thus, the density $n(r)$ for $1p$-shell nuclei has the form

$$n_{ij}(r) = \frac{16}{\sqrt{\pi}}\frac{\Gamma\left(\frac{5A-11}{2}\right)}{\Gamma\left(\frac{5A-14}{2}\right)}\int_r^\infty \frac{(\rho^2-r^2)^{\frac{5A-16}{2}}}{\rho^{5A-13}}\chi_i(\rho)\chi_j(\rho)\,d\rho$$

$$+\frac{8}{3}\frac{(A-4)}{\sqrt{\pi}}\frac{\Gamma\left(\frac{5A-11}{2}\right)}{\Gamma\left(\frac{5A-16}{2}\right)}\int_r^\infty \frac{r^2(\rho^2-r^2)^{\frac{5A-18}{2}}}{\rho^{5A-13}}\chi_i(\rho)\chi_j(\rho)\,d\rho, \qquad (13)$$

and the mean-square radius is written as

$$\bar{R}_{ii}^2 = \langle r_{ii}^2\rangle = \frac{\int n_{ii}(r)\,r^2\,dV}{\int n_{ii}(r)\,dV} = \frac{\int n_{ii}(r)\,r^4\,dr}{\int n_{ii}(r)\,r^2\,dr}, \qquad (14)$$

where the nuclear density is normalized as follows:

$$4\pi\int n(r)\,r^2\,dr = A. \qquad (15)$$

The monopole isoscalar sum rule can be written as

$$\sum_n (E_n - E_0)\mid M_{0n}\mid^2 = \frac{\hbar^2 Z}{m}\langle 0\mid r^2\mid 0\rangle = \sum_n S_{0n}, \qquad (16)$$

where

$$M_{0n} = \langle 0\mid 1/2\sum_{i=1}^{A} r_i^2\mid 0_n\rangle. \qquad (17)$$

Nuclear densities in the quasiparticle-phonon model

The densities for heavy nuclei were constructed in the framework of the quasiparticle-phonon model.[10] The most general form of the Hamiltonian of this model is

$$H = H_{\text{av}} + H_{\text{pair}} + H_M + H_{SM}, \qquad (18)$$

where H_{av} describes the independent motion of the nucleons in the average field, H_{pair} the pairing forces acting only between neutrons and protons, and H_{M} and H_{SM} the separable multipole and spin-multipole interactions that generate the nuclear excitations. The explicit form of the Hamiltonian (18) can be found, for example, in Ref. 12. All the terms in (18) make contributions when the nuclear transition densities are constructed. In the ground-state density, the contributions of H_{M} and H_{SM} are absent, and for this case we obtain the expression

$$H_0 = H_{\text{av}} + H_{\text{pair}} = \sum_{jm\tau} E_j a_{jm}^+ a_{jm}$$

$$-\sum_{\tau jj'mm'}\frac{G_\tau}{4}(-1)^{j-m+j'-m'}a_{jm}^+a_{j-m}^+a_{j'-m}a_{j'm'}, \qquad (19)$$

where a_{jm}^+ and a_{jm} are the operators of creation and annihilation of a nucleon in the level of the average field with quantum numbers $(n, j, l)\equiv j$ and angular-momentum projection m, τ is the isotopic index ($\tau = n, p$), E_j are the single-particle energies, and G_N and G_Z are the constants of the monopole pairing. For the determination of the single-particle basis, the average field is chosen in the form of the Woods–Saxon potential. The parametrization of the potential used in the framework of the quasiparticle-phonon model is given in detail in Ref. 13.

After transition to quasiparticles by means of the Bogo-

lyubov transformation $a_{jm} = u_j \alpha_{jm} + (-)^{j-m} v_j \alpha^+_{j-m}$, where α^+_{jm} and α_{jm} are the operators of creation and annihilation of quasiparticles, the following expression is obtained for the densities of the ground states of heavy (spherical) nuclei:

$$\rho_0(r) = \frac{1}{4\pi} \sum_j (2j+1) \left| \frac{R_j(r)}{r} \right|^2 v_j^2, \tag{20}$$

where $R_j(r)/r$ is the radial dependence of the wave function of the single-particle state $j \equiv (n, l, j)$. In these calculations, normalized nuclear densities are taken, the normalization condition being

$$4\pi \int \rho_0(r)\, r^2\, dr = A, \tag{21}$$

where A is the mass number of the nucleus.

We now discuss the method of constructing the nuclear potential using these densities.

Nuclear interaction potentials of heavy ions

Among the most popular methods of constructing nuclear interaction potentials of heavy ions are the folding model[14–16] and the energy-density formalism.[17]

There has been much recent development of theoretical approaches to the construction of the potentials of the interaction of nucleons, α particles, and heavy ions with nuclei in which the interaction potential is constructed on the basis of information on the effective nucleon-nucleon forces and the matter distribution in the incident and target particles.[18–27] This makes it possible to avoid the ambiguities in the description of scattering cross sections inherent in the ordinary optical model and to develop a systematic scheme for analyzing experimental data unencumbered with a large number of adjustable parameters. In the framework of these approaches, it is possible to take into account the effects of nuclear saturation,[27] the dependence of the effective forces on the density,[27,28] and the antisymmetrization.[25–27] However, in the calculations various approximations are made. The imaginary part of the nuclear interaction potential, which takes into account the coupling to the various reaction channels, is approximated by the phenomenological Woods–Saxon potential,[14] the densities of the colliding ions are simulated by all possible functions,[28] etc. Among the systematic microscopic schemes for constructing the nuclear interaction potential we must mention the work of Faessler's group,[20–24] in which the attempt is made, using the G matrix, to obtain not only the imaginary but also the real part of the heavy-ion optical potential, using, however, it must be said, the properties of infinite nuclear matter.

Below, we discuss briefly the calculation of the nuclear interaction potential of heavy ions in the folding model[14,15] and in the energy-density formalism.[17]

Folding model

The interaction potential between two nuclei or ions has not been determined. As such a potential, one uses the potential of the optical model for the system $a + A$ of two nuclei. The total wave function of the system $a + A$ is expanded with respect to the internal wave functions of the individual nuclei:

$$\Psi = \sum_{i,j} \Psi_{a_i} \Psi_{Aj} \chi_{ij}(R), \tag{22}$$

where $\chi_{ij}(R)$ describes the relative motion of the system $a + A$, nucleus a being in state i and nucleus A in state j. To elastic scattering there corresponds the wave function $\chi_{00}(R)$. If we ignore the effects of antisymmetrization between the two nuclei, whose wave functions are separately antisymmetrized, then according to Feshbach[16] the effective potential of the optical model has the form

$$U_{0n} = V_{00} + \sum_{\alpha\alpha} V_{0\alpha} \left(\frac{1}{E - H - i\varepsilon} \right)_{\alpha\alpha} V_{\alpha 0} = U_F + \Delta U, \tag{23}$$

where V is the potential of the interaction between particles a and A, and the summation is over all excited states of one or both nuclei. The first term is real and is the folding potential:

$$U_F(R) = V_{00} \equiv (\Psi_{a_0} \Psi_{A_0} \mid V \mid \Psi_{a_0} \Psi_{A_0}). \tag{24}$$

The integration in (24) is over all internal coordinates of the two nuclei. The remaining term ΔU, which takes into account the coupling to the various channels, has a dynamical nature, and to construct it the complete spectrum of excitations of the interacting nuclei must be known. In phenomenological approaches ΔU is approximated by a local complex model potential $U(R)$, for example, in the Woods–Saxon form. The parameters of the real and imaginary parts of the optical potential are frequently chosen as independent. Because of this, the range of the imaginary part of the optical potential is greater than that of the real part in the majority of cases.

The real part $U_F(R)$ of the nuclear interaction potential of the heavy ions is the averaging of the NN interaction over the densities of the two colliding particles. For this, the densities of the particles A_1 and A_2 are assumed to be unperturbed. This is justified, since the elastic scattering of heavy ions is sensitive only to the shape of the potential at a distance between the ions in the neighborhood of the critical radius[14,15]

$$R_{\text{crit}} = 1.5\,(A_1^{1/3} + A_2^{1/3}). \tag{25}$$

The densities of the colliding nuclei overlap weakly in this region, so that one can assume that their distortion is negligibly small in this case.

The double folding potential can be written in the form

$$U_F(\mathbf{R}) = \int d\mathbf{r}_1\, d\mathbf{r}_2 \rho_1(\mathbf{r}_1)\, \rho_2(\mathbf{r}_2)\, v(\mathbf{r}_{12} = \mathbf{R} + \mathbf{r}_2 - \mathbf{r}_1), \tag{26}$$

where ρ_i the is density in the ground state of nucleus i. Figure 2 shows the coordinates used in the calculations in the folding model. The expression (26) includes a six-dimensional integral.

The central part of the effective interaction is written as follows:

$$v_{12} = v_{00}(\mathbf{r}_{12}) + v_{01}(\mathbf{r}_{12})\, \tau_1\tau_2 + v_{10}(\mathbf{r}_{12})\, \sigma_1\sigma_2 + v_{11}(\mathbf{r}_{12})\, \sigma_1\sigma_2\tau_1\tau_2. \tag{27}$$

In the general case, the interaction also contains spin-orbit and tensor terms. When both interacting ions are spinless, the v_{ST} terms in the expression (27) with $S = 1$ make no

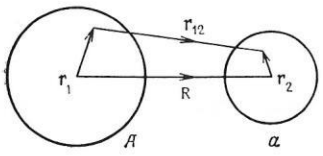

FIG. 2. Coordinates used in the double folding method.

contribution. In the general case, U_F may be nonspherical and may include terms which depend on the spins and isospins of the interacting ions. However, for the processes considered, the contribution of these terms is negligibly small.[14] Therefore, in folding calculations only the term $v_{00}(r)$ in the expression (27) is taken as the effective *NN* interaction. The radial dependence of the effective interaction is usually employed in various variants: in the form of zero-range Skyrme δ-function forces,[29] finite-range Gaussian forces of the type used by Satchler and Love,[14] and Yukawa-type forces (M3Y).[30]

For a zero-range interaction of Skyrme type the double folding potential has the form

$$U^{aA}_{ij,\,kl}(R) = \pi \int_0^{\pi} \sin\Theta\, d\Theta \left\{ \frac{3}{8} t_0 \left[\int_0^{\infty} \rho^a_{ij}(r)\, \rho^A_{kl}(|\mathbf{R}-\mathbf{r}|)\, r^2\, dr + \int_0^{\infty} \rho^A_{ij}(r)\, \rho^a_{kl}(|\mathbf{R}-\mathbf{r}|)\, r^2\, dr \right] + \frac{t_3}{16} \left[\int_0^{\infty} (\rho^a_{ij}(r))^2\, \rho^A_{kl}(|\mathbf{R}-\mathbf{r}|)\, r^2\, dr + \int_0^{\infty} (\rho^A_{ij}(r))^2\, \rho^a_{kl}(|\mathbf{R}-\mathbf{r}|)\, r^2\, dr \right] \right\}, \quad (28)$$

where $|\mathbf{R}-\mathbf{r}| = \sqrt{R^2 + r^2 - 2Rr\cos\theta}$, and t_0 and t_3 are the parameters of the two- and three-particle Skyrme interaction, respectively. For the effective *NN* potential, allowance is made here only for the spin-isospin-independent two- and three-particle terms in the Skyrme forces.[29-30]

The two-particle interaction has the form

$$v_2(\bar{r}_1 - \bar{r}_2) = t_0 \delta(\bar{r}_1 - \bar{r}_2),$$

and the three-particle forces are written as

$$v_3(\mathbf{r}_1, \mathbf{r}_2, \mathbf{r}_3) = t_3 \delta(\mathbf{r}_1 - \mathbf{r}_2)\, \delta(\bar{r}_2 - \bar{r}_3).$$

Analytic form for the folding potential with finite-range forces.[7] The analytic form of the real and imaginary parts of the optical potential makes the optical model more convenient for describing the experimental results than the ordinary variant of the folding model. Analytic expressions for the nucleon and α-particle potentials in the folding model were obtained for the first time in Refs. 31–33. In Ref. 7, this formalism was generalized for systems of interacting heavy ions. In this case, the nucleon interaction potential was chosen in Ref. 7 in Gaussian form with allowance for a soft core in the effective interaction at short distances:

$$V(r) = \sum_{k=1}^{2} V_k \exp\left(-\frac{r^2}{a_k^2}\right); \quad r = |\bar{r}_1 - \bar{R} - \bar{r}_2|. \quad (29)$$

The matter density distribution $\rho_{A(a)}(r)$ in the nucleus was also described by a Gaussian form with parameters determined from the condition of best reproduction of the nuclear densities obtained in the framework of the method of hyperspherical functions:

$$\rho_{A_i}(r) = \rho_{0i} \sum_k c_{ki} \frac{r^k}{b^k_{ki}} \exp\left(-\frac{r^2}{b^2_{ki}}\right). \quad (30)$$

Such an approximation is introduced by analogy with the analytic expression for the density in the harmonic-oscillator model, but in contrast to this model different oscillator parameters, and also terms with higher powers of r, are introduced into this formula. In the language of the shell model, this amounts to taking into account an admixture of more complicated configurations. Table I gives the parameters c_{ki} and b_{ki} of the approximation for the densities of the ground and excited states, and also the transition states with excitation of monopole resonances at energy 20 MeV of the nuclei

TABLE I. Parameters c_{ki} and b_{ki} in the approximation of the densities of the ground, ρ_{11}, and excited, ρ_{22}, states of the nuclei ^{4}He, ^{6}Li, ^{12}C, ^{16}O and also the transition densities ρ_{12} with excitation of monopole resonances.

Density	A	c_{0i}	b_{0i}	c_{1i}	b_{1i}	c_{2i}	b_{2i}	c_{3i}	b_{3i}
ρ_{11}	4	0.2560	1.3990	0.3187	0.8500	—	—	—	—
	6	0.1333	1.9800	0.6014	1.3800	—	—	—	—
	12	0.1270	2.0436	8.3435	1.7462	—	—	—	—
	16	0.1293	1.9915	13.6032	1.7553	—	—	—	—
ρ_{22}	4	0.0527	1.4574	−1.8996	1.1624	−0.4072	0.4998	0.9380	0.8778
	6	0.0608	3.1054	−5.2582	2.6661	−9.7852	1.0582	−1.0183	1.4374
	12	0.1026	2.4160	3.5108	2.1030	1.7105	0.7399	0.9628	1.0540
	16	0.1127	2.3430	9.0809	1.9188	1.6572	0.7429	0.8957	1.0239
ρ_{12}	4	0.1122	1.9190	7.8252	0.8653	−1.4145	0.5181	−0.3207	1.3875
	6	0.0527	2.8205	14.3012	1.2326	−2.0896	0.7323	−0.7558	1.8469
	12	0.0373	3.9338	1.5163	1.4238	−1.9665	0.7663	−1.8757	1.7675
	16	0.0320	4.5300	7.0300	1.4500	−1.8198	0.7510	−5.8530	1.7300

^{4}He, ^{6}Li, ^{12}C, ^{16}O as found in Ref. 34 in accordance with the expression (30).

Below, we give the expression for the spherically symmetric part of the potential $u_{A_1A_2}(\mathbf{R})$ in the case when the first three even terms are taken into account in the expansion (30):

$$
\left.
\begin{aligned}
&u_{A_1A_2}(R)=\sum_k\sum_{mn}B_k f_{km1,\,n2}(R)\exp\left(-\frac{R^2}{\delta^2_{km1,\,n2}}\right)\\
&\qquad (m,\,n=0,\,2,\,4);\\
&f_{k01,\,02}=\frac{b^3_{01}b^3_{02}}{\delta^3_{k01,\,02}};\\
&f_{k21,\,02}(R)=c_{21}\frac{b^3_{21}b^3_{02}}{\delta^3_{k21,\,02}}\left(\frac{3}{2}\frac{\mu^2_{k02}}{\delta^2_{k21,\,02}}+\frac{b^2_{21}}{\delta^2_{k21,\,02}}\frac{R^2}{\delta^2_{k21,\,02}}\right);\\
&f_{k41,\,02}(R)=c_{41}\frac{b^3_{41}b^3_{02}}{\delta^3_{k41,\,02}}\left(\frac{15}{4}\frac{\mu^4_{k02}}{\delta^4_{k41,\,02}}\right.\\
&\left.+5\frac{\mu^2_{k02}b^2_{41}R^2}{\delta^4_{k41,\,02}\delta^2_{k41,\,02}}+\frac{b^4_{41}}{\delta^4_{k41,\,02}}\frac{R^4}{\delta^4_{k41,\,02}}\right);\\
&f_{k21,\,22}(R)=c_{21}c_{22}\frac{b^3_{21}b^3_{22}}{\delta^3_{k21,\,22}}\left\{\frac{9}{4}\frac{a^2_k}{\delta^2_{k21,\,22}}\left(1+\frac{5}{3}\frac{b^2_{21}b^2_{22}}{a^2_k\delta^2_{k21,\,22}}\right)\right.\\
&\left.+\frac{3}{2}\left(1-\frac{a^2_k}{\delta^2_{k21,\,22}}-\frac{10}{3}\frac{b^2_{21}b^2_{22}}{\delta^4_{k21,\,22}}\right)\frac{R^2}{\delta^2_{k21,\,22}}+\frac{b^2_{21}b^2_{22}R^4}{\delta^4_{k21,\,22}\delta^4_{k21,\,22}}\right\};\\
&f_{k41,\,22}(R)=c_{41}c_{22}\frac{b^3_{41}b^3_{22}}{\delta^3_{k41,\,22}}\left\{\frac{45}{8}\frac{a^2_k\mu^2_{k22}}{\delta^4_{k41,\,22}}+\frac{105}{8}\frac{\mu^2_{k22}b^2_{41}b^2_{22}}{\delta^6_{k41,\,22}}\right.\\
&+\left[\frac{15}{2}\frac{a^2_kb^2_{41}}{\delta^4_{k41,\,22}}+\frac{b^2_{22}}{\delta^2_{k41,\,22}}\frac{15}{4}\left(1-\frac{14}{3}\frac{b^2_{41}}{\delta^2_{k41,\,22}}+7\frac{b^4_{41}}{\delta^4_{k41,\,22}}\right)\right]\frac{R^2}{\delta^2_{k41,\,22}}\\
&+\left[\frac{3}{2}\frac{a^2_k}{\mu^2_{k22}}\frac{b^4_{41}}{\delta^4_{k41,\,22}}+5\frac{b^2_{41}b^2_{22}}{\mu^2_{k22}\delta^2_{k41,\,22}}\left(1-\frac{14}{5}\frac{b^2_{41}}{\delta^2_{k41,\,22}}\right.\right.\\
&\left.\left.+\frac{21}{10}\frac{b^4_{41}}{\delta^4_{k41,\,22}}\right)\right]\frac{R^4}{\delta^4_{k41,\,22}}+\frac{b^4_{41}b^2_{22}}{\delta^6_{k41,\,22}}\frac{R^6}{\delta^6_{k41,\,22}}\left.\right\};\\
&f_{k41,\,22}(R)=c_{41}c_{42}\frac{b^3_{41}b^3_{42}}{\delta^3_{k41,\,42}}\left\{\frac{15}{8}\left(\frac{15}{2}\frac{a^4_k}{\delta^4_{k41,\,42}}\right.\right.\\
&\left.+35\frac{a^2_kb^2_{41}b^2_{42}}{\delta^6_{k41,\,42}}+\frac{63}{2}\frac{b^4_{41}b^4_{42}}{\delta^8_{k41,\,42}}\right)+\left[\frac{75}{4}\frac{a^2_k}{\delta^2_{k41,\,42}}\left(1-\frac{a^2_k}{\delta^2_{k41,\,42}}\right)\right.\\
&+\frac{35}{4}\frac{b^2_{41}b^2_{42}}{\delta^4_{k41,\,42}}\left(5-15\frac{a^2_k}{\delta^2_{k41,\,42}}-18\frac{b^2_{41}b^2_{42}}{\delta^4_{k41,\,42}}\right)\left.\right]\frac{R^2}{\delta^2_{k41,\,42}}\\
&+\left[\frac{15}{4}\left(1-\frac{a^2_k}{\delta^2_{k41,\,42}}\right)^2-35\frac{b^2_{41}b^2_{42}}{\delta^4_{k41,\,42}}-\frac{3}{2}\frac{a^2_k}{\delta^2_{k41,\,42}}\right)+\frac{189}{2}\frac{b^2_{41}b^2_{42}}{\delta^8_{k41,\,42}}\left.\right]\\
&\times\frac{R^4}{\delta^4_{k41,\,42}}+5\frac{b^4_{41}b^4_{42}}{\delta^4_{k41,\,42}}\left(1-\frac{a^2_k}{\delta^2_{k41,\,42}}-\frac{18}{5}\frac{b^4_{41}b^2_{42}}{\delta^4_{k41,\,42}}\right)\frac{R^6}{\delta^6_{k41,\,42}}\\
&\left.+\frac{b^4_{41}b^4_{42}}{\delta^8_{k41,\,42}}\frac{R^8}{\delta^8_{k41,\,42}}\right\};\\
&B_k=\pi^3\rho_{01}\rho_{02}V_ka^2_k;\quad \delta_{km1,\,n2}=\sqrt{a^2_k+b^2_{m1}+b^2_{n2}};\\
&\mu_{kmi}=\sqrt{a^2_k+b^2_{mi}}.
\end{aligned}
\right\}
\tag{31}
$$

There are corrections to the expression (31) associated with allowance for the Pauli principle and also second-order processes. In constructing the interaction potentials of heavy ions it is difficult to take into account exactly the antisymmetrization effects, and therefore the Pauli principle is frequently taken into account in this case by the introduction into the effective interaction of a zero-range potential.[14]

Then the radial part of the effective forces takes the form

$$
V'(S)=\sum_k V_k\exp\left(-\frac{S^2}{a^2_k}\right)+d(E)\,\delta(S). \tag{32}
$$

For the second term in (31), the structure of the expressions is basically preserved, subject to the substitutions

$$
\left.
\begin{aligned}
&B_k\to\pi^{3/2}\rho_{01}\rho_{02}d(E);\\
&a_k\to 0\mu_{kmi}\to b_{mi}\delta_{kmi,\,n2}\to\varkappa_{m1,\,n2}=\sqrt{b^2_{m1}+b^2_{n2}}.
\end{aligned}
\right\}
\tag{33}
$$

As a result, the interaction potential acquires a corresponding correction (MeV·F^3)

$$
d(E)=-276\,(1-0{,}005\,E/a). \tag{34}
$$

With regard to the second-order corrections to the potential, their contribution to the real part of the folding potential in the peripheral region is small (see, for example, Ref. 35).

Analytic forms of the folding model were also developed in Refs. 36 and 37. In Ref. 36, the formalism of the SU(3) group was used, this therefore presupposing that the harmonic-oscillator model is valid. In Ref. 37, analytic folding potentials were obtained in the cluster approximation. The representation of the density in the form (30) adopted in Ref. 7 differs from the harmonic-oscillator representation and does not use the assumption of clustering of the nucleus.

Folding potential for nucleon-nucleon forces of Yukawa type (M3Y). The main difficulty in calculating folding potentials with the M3Y interaction of Yukawa type is that in this case it is necessary to calculate exactly the six-dimensional integral (26). This problem is extremely complicated in the coordinate representation. However, following the procedure proposed in Ref. 14, one can go over to the momentum representation and instead of the six-dimensional integral obtain as a result[9] simply a product of three one-dimensional integrals. One of them can be calculated in analytic form.

Briefly, the procedure is as follows. If the Fourier transform of the function $f(\mathbf{r})$ is $\tilde{f}(\mathbf{k})=\int d\mathbf{r}\exp(i\mathbf{kr})f(\mathbf{r})$, then $v(\mathbf{r}_{12})$ in (26) has the form

$$
v(\mathbf{r}_{12})=\frac{1}{(2\pi)^3}\int d\mathbf{k},\ v(\mathbf{k})\exp\left[-i\mathbf{k}(\mathbf{R}+\mathbf{r}_2-\mathbf{r}_1)\right] \tag{35}
$$

$$
\left.
\begin{aligned}
&U_F(\mathbf{R})=\frac{1}{(2\pi)^3}\int d\mathbf{k}\exp(-i\mathbf{kR})\,\tilde{v}(\mathbf{k})\,\tilde{\rho}_1(\mathbf{k})\,\tilde{\rho}_2(-\mathbf{k});\\
&\tilde{U}_F(\mathbf{k})=\int d\mathbf{R}\exp(i\mathbf{kR})\,U_F(\mathbf{R})=\tilde{v}(\mathbf{k})\,\tilde{\rho}_1(\mathbf{k})\,\tilde{\rho}_2(-\mathbf{k}).
\end{aligned}
\right\}
\tag{36}
$$

To solve the elastic-scattering problem, it is in practice necessary to calculate only integrals of the type

$$
\tilde{\rho}(\mathbf{k})=4\pi\int_0^\infty r^2\,dr j_0(kr)\,\rho(r), \tag{37}
$$

and the expression for $\tilde{v}(k)$ can be put in analytic form if the M3Y interaction is expressed as follows[14]:

$$v(\mathbf{r}_{12}) = 6315\ \frac{\exp(-4r)}{4r} - 1961\ \frac{\exp(-2.5r)}{2.5r} - 818\,\delta(\mathbf{r}_{12}), \tag{38}$$

where $r = |\mathbf{r}_{12}| = |\mathbf{r}_1 - \mathbf{r}_2|$.

Nuclear interaction potential of heavy ions in the energy-density formalism

In this method,[8,17] the potential of the nuclear interaction between two ions is calculated in the sudden approximation, in which it is assumed that at the instant of the collision the densities of the ions are frozen. The potential has the form

$$V(R) = \int \{\varepsilon(\rho_A + \rho_a) - \varepsilon(\rho_A) - \varepsilon(\rho_a)\}\, d\tau, \tag{39}$$

where $\varepsilon(\rho)$ is the energy functional for the corresponding system, determined as follows[17]:

$$\varepsilon(\rho) = \tau_{TF} + \rho V(\rho,\ \alpha) + \eta_0 (\nabla\rho)^2 + \frac{1}{2} e\rho_p V_e - 0.378 e^2 \rho_p^{4/3}, \tag{40}$$

where $\rho = \rho_n + \rho_p$, in which ρ_n and ρ_p are the densities of the neutron and proton components, respectively, in the nucleus, and α is the neutron excess:

$$\alpha = (\rho_n - \rho_p)/(\rho_n + \rho_p).$$

The first term in (40) is the density of the kinetic energy in the Thomas–Fermi approximation:

$$\tau_{TF} = a_k \rho^{5/3} = \frac{3}{5}\frac{\hbar^2}{2m}\left(\frac{3}{2}\pi^2\right)^{2/3}\frac{1}{2}\left[(1-\alpha)^{5/3} + (1+\alpha)^{5/3}\right]\rho^{5/3}, \tag{41}$$

where m is the nucleon mass. The functional $v(\rho, \alpha)$ corresponds to the potential energy of a particle in nuclear matter:

$$V(\rho,\ \alpha) = b_1(1 + a_1\alpha^2)\rho + b_2(1 + a_2\alpha^2)\rho^{4/3} + b_3(1 + a_3\alpha^2)\rho^{5/3}. \tag{42}$$

The gradient term in (40) takes into account the fact that the nuclear system is finite; the last two terms correspond to the direct and exchange Coulomb energies. The quantities $\{a, b\}$ are determined by fitting to the binding energy and the proton radius.

For an $N = Z$ system, the parameter $\alpha = 0$ and the density parameters in $\rho_A(r)$ and $\rho_a(r)$ are also the same. With allowance for this, the nuclear interaction potential was obtained in Ref. 8 in the form of the expression

$$V(R) = 2\pi \int_{-1}^{1} d\cos\Theta \int_0^\infty f(R,\ \Theta,\ r)\, r^2\, dr; \tag{43}$$

$$f(R,\ \Theta,\ r) = \tilde{\varepsilon}(\rho_A + \rho_a) - \tilde{\varepsilon}(\rho_A) - \tilde{\varepsilon}(\rho_a) - 2\eta_0 f_1;$$

$$f_1 = (4r^2 - R^2\cos^2\Theta)\, c_a c_A;$$

$$c_{a(A)} = -\frac{\rho_{0a}}{b_{0a}^2}\exp\left(-\frac{r_{a(A)}^2}{b_{0a}^2}\right) + \frac{c_2}{b_{0a}^2}\exp\left(-\frac{r_{a(A)}^2}{b_{2a}^2}\right)(b_{2a}^2 - r_{a(A)}^2);$$

$$|\mathbf{r}_a| = \sqrt{r^2 + \frac{R^2}{4} - \frac{1}{2} rR\cos\Theta},$$

$$|\mathbf{r}_A| = \sqrt{r^2 + \frac{R^2}{4} - \frac{1}{2} rR\cos\Theta},$$

where R is the distance between the centers of the ions, and $\tilde{\varepsilon}(\rho)$ is the corresponding functional (40) without the gradient term. In the derivation of (43), the contribution of the direct Coulomb term was not taken into account, since it is effectively included in the calculation of the reaction cross section.

Formalism for calculating elastic and inelastic cross sections of reactions with heavy ions

Nuclear interaction potentials of heavy ions obtained in the manner described above were used in Ref. 15 to calculate elastic and inelastic reaction cross sections. It was assumed that the imaginary potential must have the same form as the real potential. Therefore, calculations of the elastic cross sections were made with just one free parameter:

$$U = U_F(1 + i\beta). \tag{44}$$

The parameter β in the elastic channel was found by fitting the theoretical differential cross section to experimental data. The fitting criterion was minimization of

$$\chi^2 = \sum_i \left[\frac{\sigma_{\exp}(\theta_i) - \sigma_{\mathrm{cal}}(\theta_i)}{\Delta\sigma_{\exp}(\theta_i)}\right]^2, \tag{45}$$

where $\sigma_{\mathrm{cal}}(\theta_i)$ are the calculated differential cross sections, $\sigma_{\exp}(\theta_i)$ are the measured experimental cross sections, and $\Delta\sigma_{\exp}$ are the experimental errors.

The inelastic cross sections were calculated in the coupled-channel method. The amplitude of the imaginary part of the optical potential was assumed to be proportional to its real part and was normalized in the elastic channel.

2. RESULTS OF CALCULATIONS AND DISCUSSION

Densities of light nuclei in the method of hyperspherical functions

In Ref. 5, the method of hyperspherical functions was used to find the densities of light nuclei that describe best a set of physical quantities: the binding energy, the monopole-resonance excitation energy, the mean-square radius, and the elastic and inelastic (with excitation of the monopole resonance) form factors of the studied nuclei. There now follows a brief review of the main results obtained in Ref. 5.

The expression for the elastic and inelastic form factors in the high-energy approximation[38] has the form

$$F_{ij} = 2\pi i q \sum_{\varepsilon=\pm 1} \varepsilon \int_0^\infty \frac{G_{ij}(x,\ \varepsilon)}{\tilde{q}^2(x,\ \varepsilon)} \times \exp\{i[qx\varepsilon + \Phi(x,\ \varepsilon)]\}\, n_{ij}(x)\, x\, dx, \tag{46}$$

where the functions G, $\tilde{q}$, and Φ take into account the distortion of the electron wave by the Coulomb field of the nucleus and are given in the review of Ref. 38. In the Born approximation, $G = 1$, $\Phi = 0$, $\tilde{q} = q$. The expression (46) is valid for $qR \gg 1$, $Y(0)/E \ll 1$, $E^* < E$, where $V(0)$ is the Coulomb potential at the center of the nucleus, and E^* is the energy loss of the electron. In this case, the scattering cross section has the form

$$\left(\frac{d\sigma}{d\Omega}\right)_{ij} = \left(\frac{d\sigma}{d\Omega}\right)_{\mathrm{Mott}} f_{\mathrm{rec}}\, \frac{2J_j + 1}{2J_i + 1}\, |F_{ij}|^2, \tag{47}$$

where

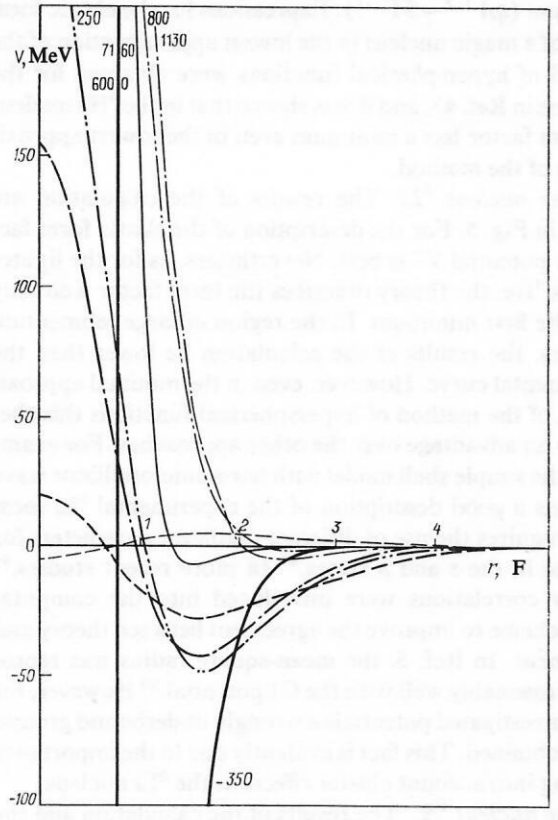

FIG. 3. Central effective potentials from Refs. 39 and 40. The continuous curve represents B4,[39] the chain curves with one and two dots C1 and B1, respectively,[39] and the broken curve the potential V7.[40] The corresponding potentials for the odd states are shown by the thin curves.

$$\frac{d\sigma}{d\Omega_{\text{Mott}}} = \left(\frac{Ze^2}{2E}\right)^2 \frac{\cos^2\frac{\theta}{2}}{\sin^4\frac{\theta}{2}} \tag{48}$$

is the Mott cross section of electron scattering by a point nucleus Z,

$$f_{\text{rec}} = \left(1 + \frac{2E}{M}\sin^2\frac{\theta}{2}\right)^{-1} \tag{49}$$

is a factor that takes into account the nuclear recoil, M is the mass of the nucleus, and J_{ij} is the spin of the initial (final) state of the nucleus.

In Ref. 5, calculations were made of the properties of light nuclei for 16 Brink–Boeker[39] and Volkov potentials.[40] Figure 3 shows the potentials[39,40] that give the best agreement in these calculations for the set of experimental data. The continuous curve represents the potential B4 (Ref. 39) with a very strong (~7000 MeV) core and a deep (~350 MeV) well; it is fairly narrow (~2 F). The chain curves with one and two dots represent, respectively, the potentials B1 and C1 with a core of order 200 MeV, well depth of about 50 MeV, and width of about 3 F. The potentials B1 and C1 differ only in the exchange variant of the forces—in the potential C1 the contribution from the even states is less and from the odd states is greater. (The potentials for odd states are shown by the thin curves.) Finally, the broken curve shows one of the Volkov potentials[40]: V7; it has a low core (~20 MeV), a shallow (~25 MeV) but broad (4–5 F) well, and a contribution of odd states, $V_{12}^H = -0.2V_{12}^4$, different from that of the previous potentials. A comparison of the results of calculations with experiment was made for the nuclei ^{4}He, ^{6}Li, ^{12}C, and ^{16}O. The reason for this choice is that

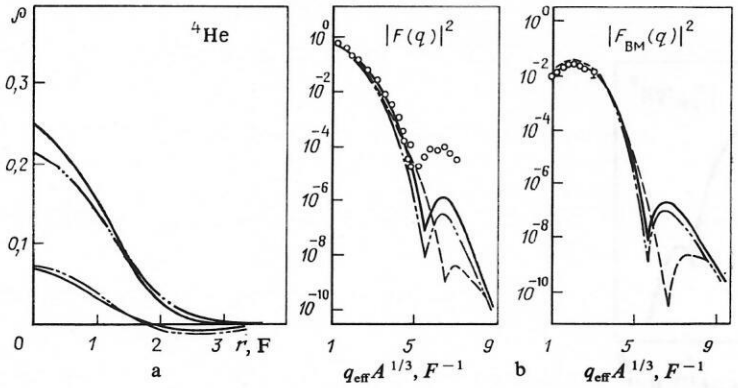

FIG. 4. Results of calculation and corresponding experimental data for the ^{4}He nucleus: the binding energy E_{bd}, the excitation energy $E_{\text{ex}}^{0^+}$ of the monopole resonance, the rms radius $\bar{R}$, and the position $qA^{1/3}$ of the minimum of the form factor for four different nucleon-nucleon potentials: a) densities of the ground and transition densities with excitation of the monopole resonance for two forms of potential; b) elastic and inelastic form factors for the same potentials. The points represent the experimental data.

Parameters	Experiment	B1	B4	V7
E_{CB}, MeV	28.3	29.3	33.4	28.0
$E_{\text{B}}^{0^+}$, MeV	20.2	26.4	31.4	24.4
$\bar{R}$, F	1.482	1.728	1.607	1.725
$qA^{1/3}$, F^{-1}	5	5.4	5.5	6.5

for them experimental data are known for the elastic form factors; for the nucleus ^{4}He, the position of the monopole 0^+ state and its elastic form factor are known; and for the ^{12}C nucleus the position of the high-lying monopole 0^+ state is known.

The nucleus ^{4}He. Figure 4 shows the results of calculating the binding energy, the excitation energy of the monopole resonance, the mean-square radius, and the position of the minimum in the form factor for various *NN* potentials. The first column of the accompanying table gives the corresponding experimental data. The experimental mean-square radii were obtained by the method of model-independent analysis of the form factors of elastic electron-nucleus scattering with separation of the proton sizes.[41]

Figure 4a shows the densities of the ground and transition densities with excitation of the monopole resonance for two forms of the potential. Figure 4b gives the results of calculation of the elastic and inelastic form factors for the same potentials. The points show experimental results.[42] Among the tested class of potentials, the best for describing the investigated phenomena for this nucleus is B1. It gives values for the binding energy, monopole-resonance excitation energy, and mean-square radius that are larger than the experimental values. However, among the potentials employed it is difficult to find one that describes the set of phenomena better. Indeed, for potentials with a larger core and deeper well, B4, the mean-square radius is reduced but there is a considerable increase in the binding energy of the ground state and the excitation energy of the monopole resonance. If potentials of Volkov type[40] are included in the calculational scheme, the theory reproduces well the binding energy and the position of the 0^+ level. However, the minimum of the form factor is shifted to the right strongly. For all the potentials, the elastic form factor is well described as far as the first minimum ($qA^{1/3} \sim 5\ \mathrm{F}^{-1}$). Expressions for the elastic form factor of a magic nucleus in the lowest approximation of the method of hyperspherical functions were obtained for the first time in Ref. 43, and it was shown that in the ^{4}He nucleus the form factor has a minimum even in the lowest approximation of the method.

The nucleus ^{6}Li. The results of the calculation are shown in Fig. 5. For the description of the elastic form factor, the potential V7 is best. Nevertheless, as for the lighter nucleus ^{4}He, the theory describes the form factor well only up to the first minimum. In the region of large momentum transfers, the results of the calculation lie lower than the experimental curve. However, even in the minimal approximation of the method of hyperspherical functions this theory has an advantage over the other approaches. For example, in the simple shell model with harmonic-oscillator wave functions a good description of the experimental ^{6}Li form factor requires the use of different oscillator parameters for particles in the *s* and *p* states.[44] In more recent studies,[45] Jastrow correlations were introduced into the computational scheme to improve the agreement between theory and experiment. In Ref. 5, the mean-square radius was reproduced reasonably well with the C1 potential.[39] However, for all the investigated potentials a strongly underbound ground state is obtained. This fact is evidently due to the importance of taking into account cluster effects in the ^{6}Li nucleus.

The nucleus ^{12}C. The results of the calculation and the corresponding experimental data are given in Fig. 6. For this nucleus, the theory with the potential B4 gives good agreement with experiment for the elastic form factor in a wide range of momentum transfers. There is a depression of the density at the center of the nucleus due to manifestation of shell effects, which increase the contribution of the *P* state. With regard to the binding energy and the mean-square radi-

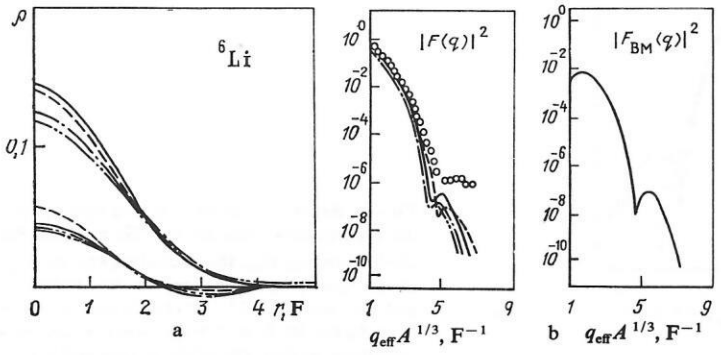

FIG. 5. The same results for the nucleus ^{6}Li.

Parameters	experiment	V7	B1	C1	B4
E_{bd}, MeV	31.99	19.8	18,2	15.9	19,5
E_{ex}^{0+}, MeV	–	14,7	15,0	14,3	17,8
$\overline{R}$, F	2.353	2,325	2,424	2,382	2,253
$qA^{1/3}$, F^{-1}	5	5	4,3	4,5	4,5

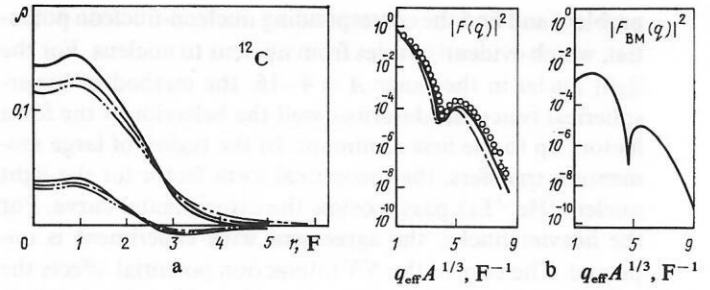

FIG. 6. The same results for the nucleus ^{12}C.

Parameters	experiment	B1	C1	B4	V7
E_{bd}, MeV	92.2	62,5	57,5	69.2	83.1
E_{ex}^{0+}, MeV	20.3	20.3	20.5	25,3	21,5
$\overline{R}$, F	2.294	2.634	2,585	2.460	2,325
$qA^{1/3}$, F^{-1}	4,1	3.9	3.9	4,1	—

us, an underbound ground state and excessively large mean-square radius are obtained to greater or lesser degrees for the investigated potentials. This result is obviously due to an inadequate choice of the nuclleon-nucleon potential. Indeed, as was shown in Ref. 46, the theory gives an overbound ground state and a mean-square radius too small in calculations for the ^{12}C nucleus with central potentials of a rectangular well and of Yukawa type.

The nucleus ^{16}O. Figure 7 shows the results of the calculations and the corresponding experimental values for the ^{16}O nucleus. It can be seen that the theory with the potential B1 reproduces well the experimental value of the form factor in a wide range of momentum transfers as far as the second minimum ($qA^{1/3} \sim 9$ F^{-1}). It is natural to ask how these properties are changed when allowance is made for higher configurations. The characteristics of the ^{16}O nucleus were investigated in the orthogonal-scheme model in Ref. 47. It was found that all the results of this model are close to those of the method of hyperspherical functions with the same number of harmonics taken into account if the parameter of the model is chosen in accordance with the variational procedure. It was shown that in the minimal-harmonic approximation the second diffraction minimum of the charge form factor in the investigated region of momentum transfers can-

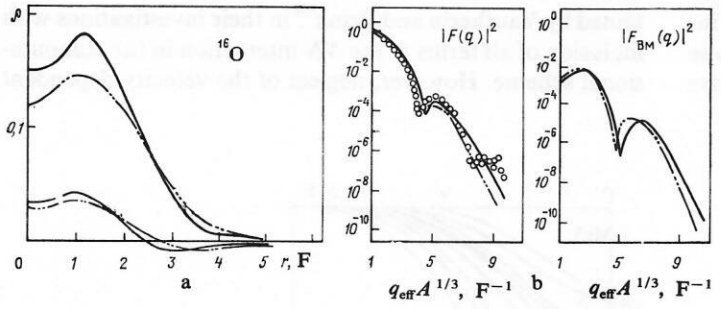

FIG. 7. The same results for the nucleus ^{16}O.

Parameters	experiment	B4	B1	V7
E_{bd}, MeV	127.2	122.2	106.31	146.5
E_{ex}^{0+}, MeV	—	29,1	22,9	25,4
$\overline{R}$, F	2.541	2,460	2.66	2,202
$qA^{1/3}$, F^{-1}	4	4,4	4	—

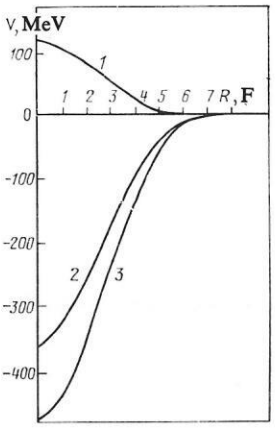

FIG. 8. Folding potential for the ^{16}O–^{16}O system for Skyrme δ-function forces (curve 2). Curves 1 and 3 are the contributions from the terms with amplitudes t_3 and t_0, respectively.

not be obtained. But this can be done if allowance is made for four harmonics with $K = K_{min} + 2$ and the most symmetric spatial Young diagrams, though even in this case the complete behavior of the curve cannot be matched. With regard to the breathing excitations, they change little when the hyperspherical basis is extended and can be satisfactorily described already in the minimal-harmonic approximation.

Besides this, study of the contribution of various nucleon states to the density distribution of the ground states of the nuclei ^4He, ^{16}O, ^{40}Ca in the method of hyperspherical functions[48] indicated that the contribution of the higher harmonics to the matter distribution in the nucleus is important only near the boundary of the nucleus.

Taken together, the results of the calculations of Ref. 5 permit some general comments to be made. Among the investigated central effective potentials [39,40] there are some that satisfactorily describe the set of phenomena for the light nuclei: the binding energy, the monopole-resonance excitation energy, the mean-square radius, and the elastic and inelastic form factors. In order to reproduce in detail these data for each nucleus, it is necessary to solve the inverse problem and find the corresponding nucleon-nucleon potential, which evidently varies from nucleus to nucleus. For the light nuclei in the range $A = 4-16$, the method of hyperspherical functions describes well the behavior of the form factors up to the first minimum. In the region of large momentum transfers, the theoretical form factor for the light nuclei (^4He, ^6Li) passes below the experimental curve. For the heavier nuclei, the agreement with experiment is improved. The core in the *NN* interaction potential affects the behavior of the form factor in the region of large momentum transfers. The larger the core, the higher the form factor in this region.

Thus, in Ref. 5 the method of hyperspherical functions was used to obtain the densities of the nucleon distributions for a number of light nuclei, and these were tested on a set of experimental data.

On the nuclear interaction potential in reactions with heavy ions

Folding potentials with zero-range forces

The densities obtained in Ref. 5 for the light nuclei were subsequently included in the scheme for calculating the nuclear interaction potential in reactions with heavy ions.[49,50] Numerical calculations were made for the nuclei ^4He, ^6Li, ^{12}C, ^{16}O. Density-dependent Skyrme δ-function forces[29] were used for the *NN* interaction. A study was made of the influence of a number of effects on the results of the calculation: three-particle forces in the *NN* interaction, the dependence of the folding potential on the number of particles, and the manifestation of the symmetry of the potential in the interaction of identical and different nuclei. Interaction potentials of heavy nuclear particles were constructed for both ground states and monopole-excited states of the nuclei, and these made it possible to describe inelastic processes.

In Refs. 49 and 50, the values 1057.3 and 14 463.5 MeV/F^3, respectively, were used for the parameters t_0 and t_3 in the Skyrme δ-function forces. These parameters were obtained by Vautherin and Brink[29] in their investigations with inclusion of all terms of the *NN* interaction in the computational scheme. However, neglect of the velocity-dependent

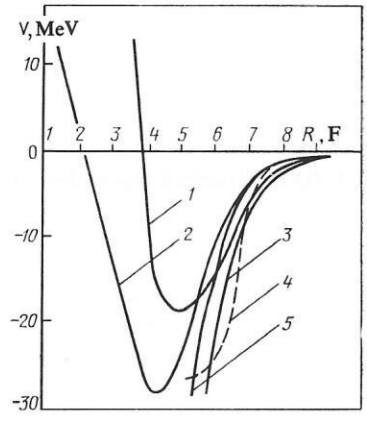

FIG. 9. Comparison of results of a calculation[50] of the ^{16}O–^{16}O folding potential (curve 5) with a phenomenological potential (curve 4), and also with the results of other theoretical studies (curves 1–3) from Ref. 52.

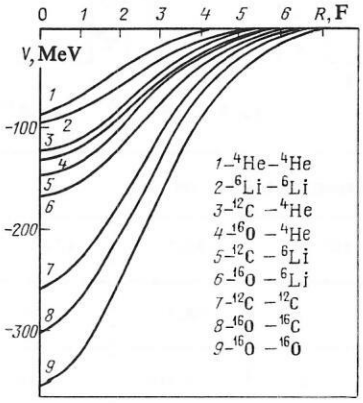

FIG. 10. Folding potentials for different combinations of nuclei with $A = 4, 6, 12, 16$.

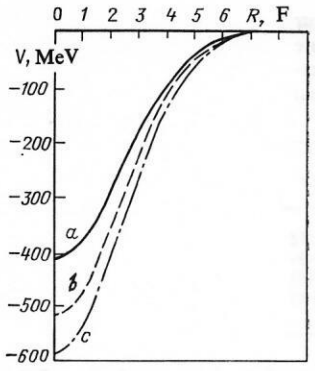

FIG. 11. Folding potential for the ^{16}O–^{16}O system with Skyrme δ-function forces for the three sets of parameters t_0 and t_3 in Table II [a) continuous curve; b) broken curve; c) chain curve].

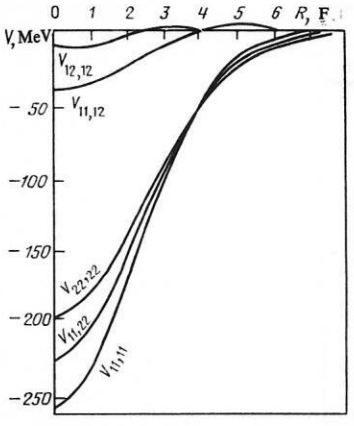

FIG. 12. Folding potentials for the ^{12}C–^{12}C system in the ground and monopole-excited states: one of the nuclei in the monopole-excited state, $V_{11,22}$; both nuclei in the monopole-excited state, $V_{22,22}$. Also, the nondiagonal matrix elements $V_{11,12}$ and $V_{12,12}$ describing the interaction between them.

terms without corresponding renormalization of the parameters t_0 and t_3 (as was done in Ref. 50) does not significantly change the properties of the nuclear ground states.[51] In addition, as was shown in Ref. 52, the properties of the nuclear ground state can be described correctly with parameters close to those used in Refs. 49 and 50 (in the simple variant of Skyrme δ-function forces—without allowance for velocity-dependent terms).

The results of the calculation of Ref. 50 are shown in Figs. 8–11. Figure 8 gives the results of the calculation for the ^{16}O–^{16}O system with and without allowance for the term corresponding to the three-particle forces in the *NN* interaction. It can be seen that this term makes an important contribution to the interaction potential of two heavy particles for distances between them up to 6 F. The critical radius in this case is equal to 7.5 F. This suggests that in the elastic scattering of ^{16}O nuclei the three-particle forces in the *NN* interaction will be weakly manifested.

In Fig. 9, the folding potential from Ref. 50 for the ^{16}O–^{16}O system is compared with the results of other theoretical studies[52] and with a phenomenological potential.[52] One can say that the folding potentials obtained in Ref. 50 are in satisfactory agreement with the results of the other theoretical investigations in the range of distances 6–9 F between the interacting nuclei. However, for a more detailed analysis it is necessary to test the calculated potential directly in elastic-scattering reactions with heavy ions.

Further, in Ref. 50 the dependence of the folding potential on the number and type of interacting particles was investigated. Figure 10 gives the results of the calculation for different combinations of nuclei with $A = 4, 6, 12, 16$. It can be seen that the potential becomes deeper and broader with increasing number of interacting particles in the dependence $A_1A_2/(A_1 + A_2)$, with the result that the (^{16}O, ^4He) interaction potential is shallower than the one for (^{12}C, ^6Li).

The dependence of the folding potential on the choice of the *NN* interaction parameters t_0 and t_3 in the Skyrme δ-function forces was investigated in Ref. 8. Figure 11 gives the results of the calculation of the nuclear interaction potential for the ^{16}O–^{16}O system. The calculations were made for three sets of parameters t_0 and t_3. The values of these parameters are given in Table II. The variants *a*, *b*, *c* differ in the contribution of the three-particle forces determined by the parameter t_3. The calculations of Ref. 8 showed that with increasing ratio t_0/t_3 the resultant folding potential becomes deeper. Thus, the increased contribution of the three-particle forces, which are repulsive in nature, decreases the depth of the nuclear interaction potential. The microscopic approach presented here can be used with equal success to construct folding potentials for systems in excited states. Such investigations were made in Refs. 1 and 2. In particular, folding potentials were calculated for monopole-excited states of the ^{12}C nucleus. The results of the calculations are shown in Figs. 12 and 13.

The calculations of the folding potentials for the monopole-excited states of the nuclei showed that the potentials are broader and shallower, the higher the nuclear excitation energy. The nondiagonal matrix elements are not negligibly small. These investigations are of particular interest, since the question of experimental detection of giant monopole

TABLE II. Parameters of Skyrme potentials.

Variant of *NN* potential	t_0	t_3	t_0/t_3	V, MeV, $R = 0.1$ F
a	−1057,3	14464,5	0,073	−410,25
b	−1170	9331,0	0,125	−522,75
c	−1205,6	5000,0	0,241	−586,2

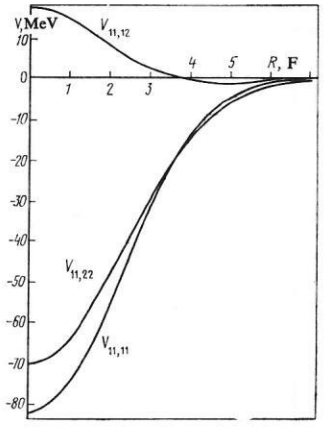

FIG. 13. Folding potentials for the ^{3}He–^{12}C system in the ground and monopole-excited states: nucleus in the ^{12}C monopole-excited state, $V_{11,22}$; both nuclei in the ground state, $V_{11,11}$; the nondiagonal matrix element $V_{11,12}$ corresponding to the interaction between them.

resonances in light nuclei ($A \leqslant 16$) has still not been unambiguously resolved.

However, the method of hyperspherical functions should give reliable theoretical predictions in the description of monopole vibrations of nuclei; for the wave function of the breathing mode is the next solution of the same equation as for the ground state, and the unfreezing of a degree of freedom such as the collective variable ρ makes it possible to take into account correctly the effect of the increased size of the nucleus in the excited state. Therefore, if the folding potential for the ground state satisfactorily describes the experimental data, reliable theoretical predictions on the properties of the monopole resonance should be obtained.

TABLE III. The parameters that occur in the expression (50) and approximate the densities of light nuclei as constructed in the method of hyperspherical functions.

A	ρ_0, F^{-3}	b_0, F	b_2, F	c_2
^{4}He	0.256	1.400	0.850	0.082
^{6}Li	0.133	1.870	1.380	0.080
^{12}C	0.127	2.040	1.750	1.060
^{16}O	0.129	1.990	1.750	1.770

Folding potentials and effective finite-range nucleon-nucleon forces.[7] Whereas the density of the matter distribution in a nucleus can be fairly reliably established in a number of cases by theoretical or experimental methods, the choice of the effective *NN* interaction contains a certain arbitrariness. The most reliable information on the *NN* interaction is obtained from analysis of free *NN* scattering. However, the vacuum *NN* interaction is strongly modified in a system such as a nucleus. In the framework of the theory of nuclear matter, the so-called realistic M3Y interaction was constructed in Ref. 30 from the vacuum nucleon-nucleon forces, and it

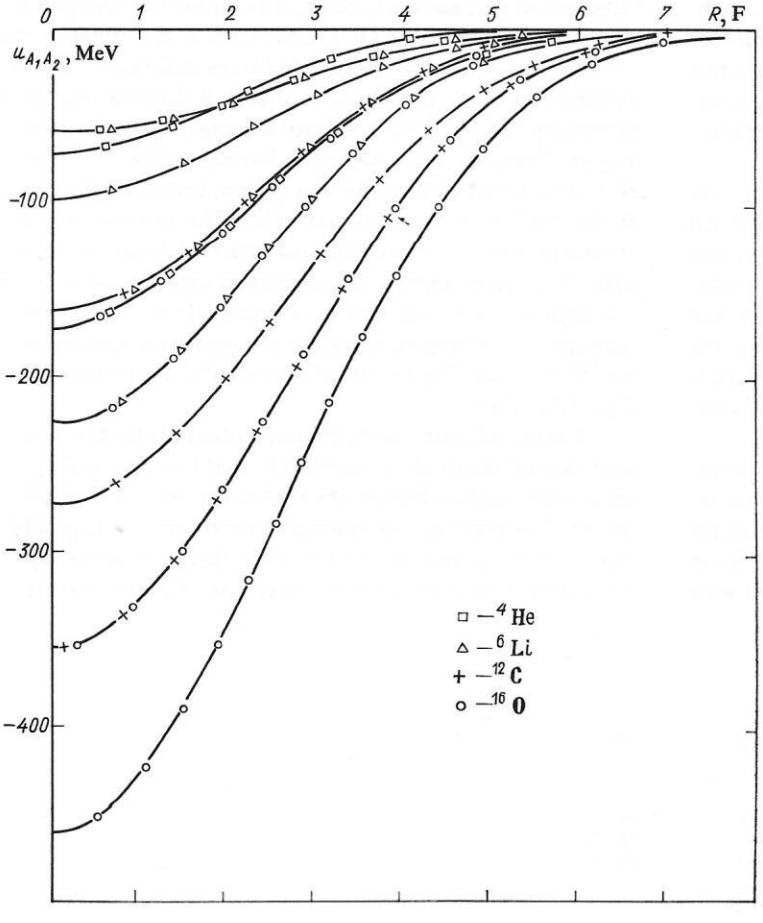

FIG. 14. Folding potentials for systems containing the ions ^{4}He, ^{6}Li, ^{12}C, ^{16}O.

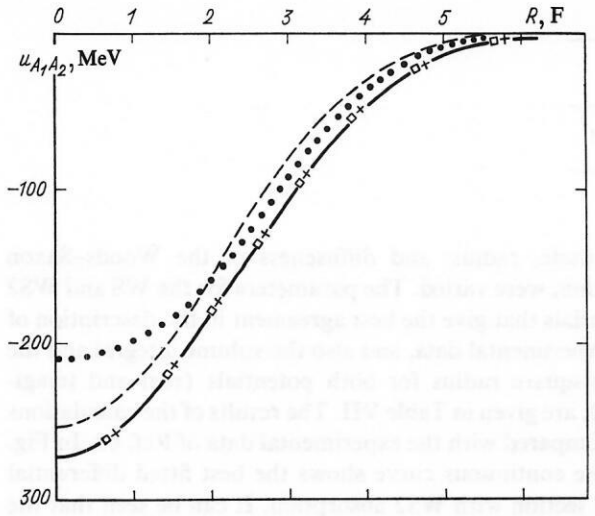

FIG. 15. Folding potentials for the ^{4}He–^{12}C system: dotted curve for the phenomenological Woods–Saxon potential, dashed curve for the Skyrme δ-function forces, and the remaining curve for Satchler–Love Gaussian-type forces.

was successfully tested on the description of the elastic scattering of heavy ions.[14] In some cases, it is convenient to represent the M3Y interaction in the form (29), renormalizing the Yukawa radial dependence into a Gaussian dependence. Then in accordance with Refs. 32 and 33 the values given in Table VI are obtained for the interaction parameters.

Folding potentials for systems containing the ions ^{4}He, ^{6}Li, ^{12}C, and ^{16}O were constructed in Ref. 7 in accordance with the expressions (31) on the basis of finite-range effective forces with these parameters. For the densities of the matter distribution in the ions, a particular form of the expression (30) was used in this case:

$$\rho(r)=\rho_0\left[\exp\left(-\frac{r^2}{b_0^2}\right)+c_2\frac{r^2}{b_2^2}\exp\left(-\frac{r^2}{b_2^2}\right)\right]. \qquad (50)$$

Table III gives the parameters that occur in the expression (50) as constructed in the method of hyperspherical functions; they were found by the least-squares method and approximate the densities of the light nuclei with high accuracy. The results of the calculation of Ref. 7 are given in Fig. 14, and more complete results for the ^{4}He + ^{12}C system are also given in Fig. 15 and in Table IV.

Some characteristic features of folding potentials were noted in the review of Ref. 14. The results given in Figs. 14 and 15 reflect these features. The folding potentials are deep, and their value at $R=0$ is given by the expression $A_1J'_{00}\rho_2(R=0)$, where J'_{00} is the strength of the two-particle effective forces, up to a factor 2 for all the systems considered. The shape of the potentials differs from the radial dependence of the Woods–Saxon potential. The results of the calculation given in Fig. 15 showed that the folding potential is appreciably deeper than the optical-model potential used in Ref. 53 to analyze the angular distributions of 139-MeV α particles elastically scattered by ^{12}C. In the surface region, the behavior of the two curves is the same, though the value of the folding potential is somewhat higher than that of the optical potential. As follows from Table IV, the radii of decrease to the 50% level and the strengths of the theoretical and phenomenological potentials differ by 9 and 16%, respectively. In Ref. 1, folding potentials with a Skyrme interaction were calculated. The corresponding result for the ^{4}He–^{12}C system is given in Fig. 15. The curves corresponding to the Skyrme *NN* interaction and finite-range forces are similar for the complete region of the nucleus. However, as was to be expected, the 50%-decrease radius is somewhat smaller for the Skyrme interaction, and the strength of the potential is 20% smaller in this case.

TABLE IV. Radii of 50% decrease and strength of the theoretical and phenomenological potentials for the ^{4}He–^{12}C system.

Parameter	$u_{sk}(r)$	$u_{\text{real}}(r)$	$u_{\text{opt}}(r)$
$R_{1/2}$, F	2.40	2.56	2.80
$J/4A$, MeV · F^3	323	406	353

In Ref. 8, in which microscopic densities obtained in the method of hyperspherical functions were used, nuclear interaction potentials of the ^{16}O–^{16}O system were constructed in two different models: in the folding model and in the energy-density formalism. A study was made of the effect on the results of the calculation of the shape of the effective *NN* interactions, the choice of the distribution density, and also the effect of antisymmetrization of the colliding nuclei. The results of the calculation are given in Fig. 16. The parameters of the potential in the case of the energy-density formalism are given in Table V, and in the case of the folding model with finite-range forces in Table VI.

The calculation shows that the depth of the interaction potential is determined by the choice of the density of the colliding ions—the increase in the density at short distances

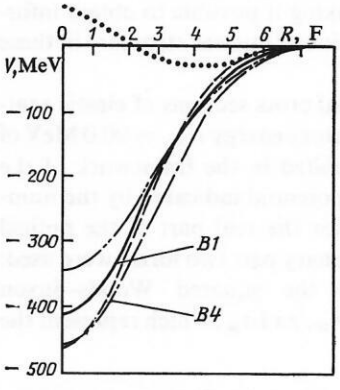

FIG. 16. Potentials of the ^{16}O–^{16}O nuclei in the energy-density formalism (points), in the folding-model method with Skyrme δ-function forces (the continuous curve corresponds to the nuclear interaction potential calculated with densities obtained in the method of hyperspherical functions with the parameter set B1, while the broken curve corresponds to the set B4), with finite-range forces with effective allowance ($DL\neq 0$, chain curve with one dot) and without allowance ($DL=0$, chain curve with two dots) for antisymmetrization.

TABLE V. Parameters of the potential (42) in the energy-density formalism.

b_1	b_2	b_3	a_1	a_2	a_3	η_0
−588.75	563.56	160.92	−0,424	−0.0973	−2,25	7,23

for the B4 set compared with the B1 set leads accordingly to a deeper nuclear interaction potential. The folding potential with finite-range forces is characterized by a stronger interaction at large R than for the result obtained when zero-range forces are used. In particular, the nuclear interaction potential obtained with the B1 set and Skyrme δ-function forces (variant a; see Table II) has the value $V(R_{cr}) = 1.05$ MeV at the point of the critical radius, whereas for the finite-range forces $V(R_{cr}) = -2.74$ MeV. Allowance for the effect of antisymmetrization in the calculation with finite-range forces leads to an increase in the depth of the potential at all values of R. The nuclear interaction potential obtained in the energy-density formalism is characterized by a repulsive core up to $R \approx 2.2$ F. Its maximal depth, $V_0 = -31.35$ MeV at $R = 4.1$ F, is appreciably less than in the other cases. Thus, the ^{16}O–^{16}O interaction potential calculated in the various models[15,17] with different effective forces differs appreciably at short distances, but in the peripheral region the difference becomes unimportant.

Study of the angular distributions of the elastic cross sections in heavy-ion reactions

In this section, we give the results of calculations in the framework of the optical model and compare them with experiment for elastic-scattering reactions in collisions of heavy ions.

A microscopic approach was used to construct the optical potential. Compared with the phenomenological[57] analysis of heavy-ion scattering, the investigation of elastic reaction cross sections in the microscopic approach[58–61] has the undoubted advantage of making it possible to obtain information about the manifestation of nuclear structure in these processes.

In Ref. 1, the differential cross sections of elastic scattering of ^{6}Li by ^{12}C for laboratory energy $E_{lab} = 90.0$ MeV of the lithium ions were calculated in the framework of the optical model. The folding potential indicated by the number 5 in Fig. 10 was used for the real part of the optical potential, while for the imaginary part two forms were used: Woods–Saxon (WS) and the squared Woods–Saxon (WS2). The parameters W, r_W, and a_W, which represent the amplitude, radius, and diffuseness of the Woods–Saxon function, were varied. The parameters for the WS and WS2 potentials that give the best agreement in the description of the experimental data, and also the volume integral and the mean-square radius for both potentials (real and imaginary), are given in Table VII. The results of the calculations are compared with the experimental data of Ref. 62. In Fig. 17, the continuous curve shows the best fitted differential cross section with WS2 absorption. It can be seen that the theoretical curves are in satisfactory agreement with the experimental data and that the differential structure is reproduced well.

In Ref. 6, a theoretical investigation was made of the elastic scattering by the ^{12}C nucleus of ^{6}Li ions with two different energies (30.6 and 90 MeV). The results of the calculation are shown in Figs. 18 and 19.

Figure 18 shows the angular distributions of ^{6}Li–^{12}C elastic scattering at 90 MeV and corresponding calculations using the microscopic NN potentials S1 and S2. Figure 19 shows the ^{6}Li–^{12}C angular distribution at energy 30.6 MeV using the NN potential S2. The imaginary part of the optical potential was chosen in the Woods–Saxon form with the parameters given in Table VIII.

It can be seen that the calculation corresponding to a decrease by 1.5 times in the amplitude corresponding to the contribution of the three-particle forces leads to a better description of the experimental data (better by 20%) at large angles, beginning with $\theta = 80°$ (Fig. 18). In addition, the results show that the potential S2 gives a qualitative description of the curves at both 30.6 MeV and 90 MeV. The nonlocality of the potential is here determined by the variation of its imaginary part. An analogous result was obtained in Ref. 62, in which a phenomenological folding potential (real part of the potential) was constructed to describe the data on ^{6}Li–^{12}C elastic scattering at 19 energies. Good agreement with the experimental data was obtained on the basis of this potential by varying its imaginary part, taken in Woods–Saxon form.

The investigations made in Ref. 6 are interesting from the point of view that in them a qualitative description can be obtained for the experimental data on ^{6}Li–^{12}C elastic scattering at the two energies 30.6 and 90 MeV with the same

TABLE VI. Parameters of the potential (29) in finite-range forces of Satchler–Love Gaussian type.

Variant of NN potential	V_1, MeV	V_2, MeV	a_1, F	a_2, F	d, MeV · F^3
1	553.18	1781.4	0.8	0.5	0
2	601.99	2256.4	0.8	0.5	$-276\,(1-0.005\,E/A)$

TABLE VII. Parameters of the imaginary part of the optical potential for the ^{6}Li–^{12}C system.[1]

Optical potential	$-W$, MeV	r_W, F	a_W, F	Volume integral, MeV · F^3	$\langle R^2\rangle^{1/2}$, F
Real "5"	—	—	—	309.6	3.53
Imaginary WS	29.8	0.915	1.157	178.1	5.18
WS2	27.4	1.262	1.200	158.2	4.47

real part of the potential without renormalization of the amplitudes in the Skyrme δ-function forces. The nonlocality of the potential is determined in this case by the decrease in its imaginary part.

The variant chosen in Refs. 1 and 6 to calculate the elastic cross sections, in which the imaginary part of the optical potential is chosen in the Woods–Saxon form, makes it possible to implement independent choice of the three parameters of the absorption potential. In this manner one can take into account the circumstance that, as a rule, the range of the imaginary part of the optical potential is greater than the radius of the real part. However, in the folding model a different way of taking into account the absorption potential is also used.[15] In this case, the shape of the imaginary part of the potential is taken to be the same as for the real part of the folding potential, and the depth of the absorption potential is regulated by a factor. In this connection, the microscopic approach under discussion was tested theoretically in all the other studies to be discussed here in accordance with the scheme in which the real and imaginary parts of the investigated potential are taken as calculated in the microscopic model, it being assumed that the imaginary potential has the same shape as the real one; only the amplitude of the forces in the imaginary part is varied [see Eq. (44)].

In this case, there is in the description of elastic scattering just one free parameter β (in contrast to the optical model with six adjustable parameters).

Figure 20 shows the results of the calculation in Ref. 2 of the ratio of the elastic-scattering cross sections to the Rutherford cross section and a comparison of these ratios with experiments.[62,63] For these three cases, the parameter β was found to be 0.7–0.9.

Despite the simplicity of the potential, used here with just one free parameter, the agreement with experiment was found to be good.

This approach was also used in Ref. 8 to analyze the differential cross sections of ^{16}O–^{16}O elastic scattering at three different energies of the incident particles: $E_{\text{lab}} = 41$, 49, and 63 MeV.[64] Figure 21 shows a comparison with experiment of the results of the calculation with an NN interaction of the type of Skyrme δ-function forces (variant a, Table II) of the differential cross sections at the three different energies. The parameter of the imaginary part of the optical potential was varied as a function of the energy of the incident ion with the aim of obtaining the best reproduction of the experimental data; the values obtained were $\beta = 0.04$, 0.1,

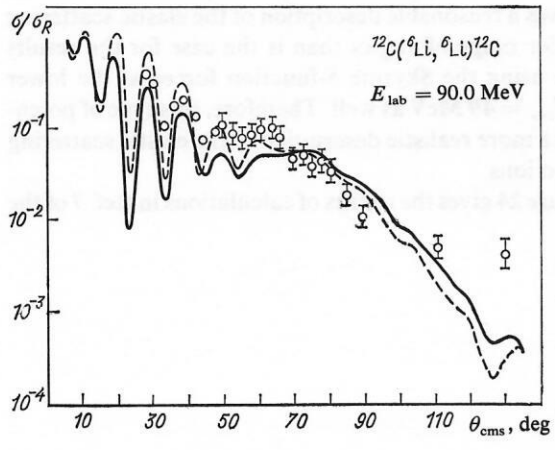

FIG. 17. Ratio of the angular distribution of elastic scattering of lithium to the Rutherford cross section in the center-of-mass system for ^{6}Li–^{12}C. The continuous and broken curves give the results of calculation in the optical model with the imaginary potentials whose parameters are given in Table VII and the real potential labeled 5 in Fig. 10.

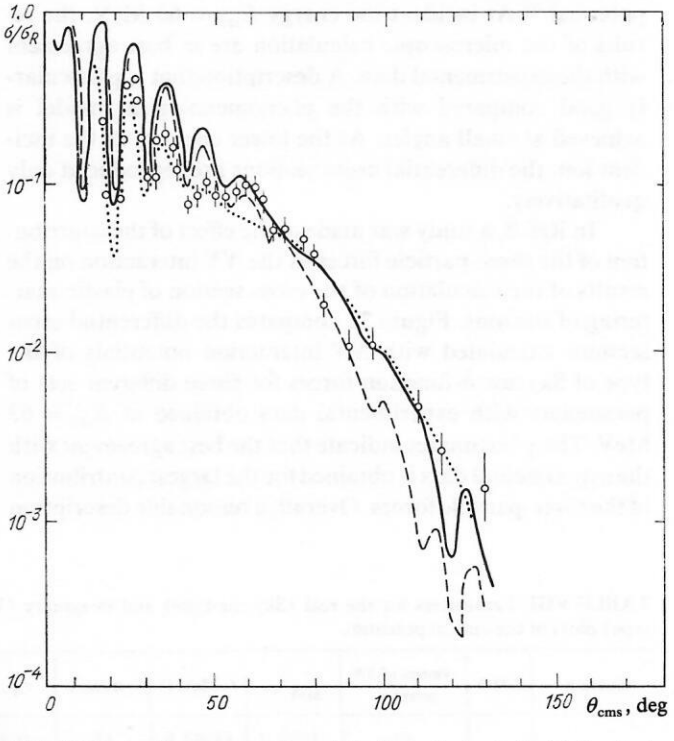

FIG. 18. Ratio of the cross sections of elastic scattering to the Rutherford cross section for ^{6}Li–^{12}C reactions at 90 MeV. The points are the experimental values of the cross sections, the broken curve gives the optical calculation using the NN potential S1, the continuous curve is the calculation corresponding to the potential S2, and the dotted curve is the one with the use of the Woods–Saxon potential.

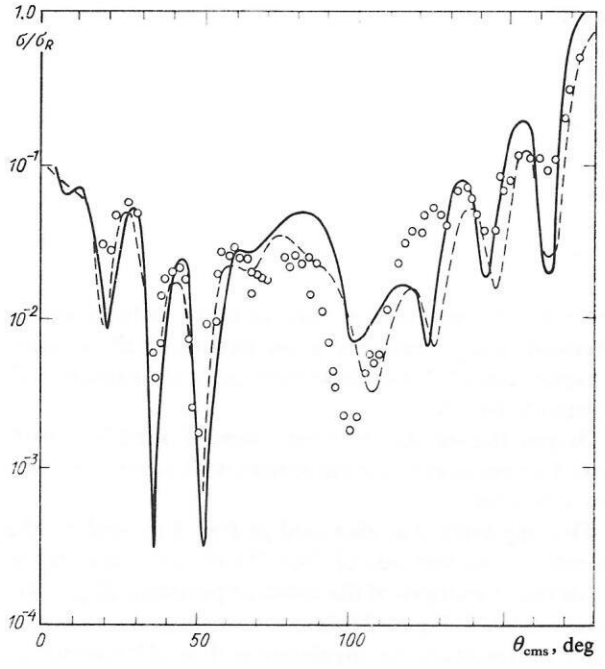

FIG. 19. Ratio of the cross sections of elastic scattering to the Rutherford cross section for ^{6}Li–^{12}C reactions at 30.6 MeV. The points are the experimental values of the cross sections, the continuous curve shows the optical calculation using the *NN* potential S2, and the broken curve shows the calculation using the Woods–Saxon potential.

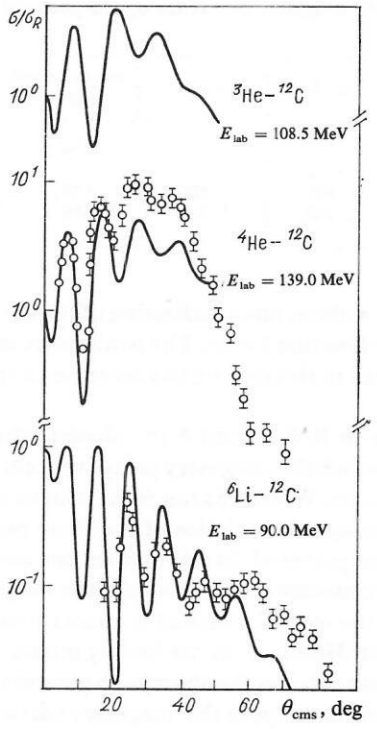

FIG. 20. Results of calculation, and comparison of them with experiment (points), of the ratio of the cross sections of elastic scattering to the Rutherford cross section for the ^{3}He–^{12}C, ^{4}He–^{12}C, ^{6}Li–^{12}C reactions.

and 0.2, respectively. The thin curve shows the results of a phenomenological calculation based on the Woods–Saxon potential.[64] At incident-ion energy $E_{lab} = 63$ MeV, the results of the microscopic calculation are in best agreement with the experimental data. A description that is particularly good compared with the phenomenological model is achieved at small angles. At the lower energies of the incident ion, the differential cross sections are reproduced only qualitatively.

In Ref. 8, a study was made of the effect of the contribution of the three-particle forces in the *NN* interaction on the results of the calculation of the cross section of elastic scattering of the ions. Figure 22 compares the differential cross sections calculated with *NN* interaction potentials of the type of Skyrme δ-function forces for three different sets of parameters with experimental data obtained at $E_{lab} = 63$ MeV. The χ^2 estimates indicate that the best agreement with the experimental data is obtained for the largest contribution of the three-particle forces. Overall, a reasonable description of the experimental data can be obtained up to scattering angles $\theta = 65°$ for $\beta = 0.2$.

In Refs. 7 and 8, elastic scattering of ions with inclusion in the computational scheme of nucleon-nucleon forces of Gaussian type as proposed by Satchler and Love was studied. For example, in Ref. 8 the differential cross sections of ^{16}O–^{16}O elastic scattering at 49 and 63 MeV were constructed and compared with experiment. The results of the calculation are shown in Fig. 23. The parameter in the imaginary part of the optical potential was found to be 0.3. It follows from Fig. 23 that the best description is obtained at the higher energy. However, the use of a potential with finite-range forces gives a reasonable description of the elastic scattering for a wider range of angles than is the case for the results obtained using the Skyrme δ-function forces at the lower energy $E_{lab} = 49$ MeV as well. Therefore, this type of potential gives a more realistic description of the elastic scattering of the two ions.

Figure 24 gives the results of calculations in Ref. 7 of the

TABLE VIII. Parameters for the real (Skyrme-type) and imaginary (Woods–Saxon-type) parts of the optical potential.

System	E, MeV	Variant of *NN* potential	$-t_0$, MeV/F^3	t_3, MeV/F^3	$-W$, MeV	r_W, F	a_W, F
^{6}Li—^{12}C	90	*S*1	1057.3	14463.5	45	0.89	0.8
		*S*2	1170.0	9331.0	48	0.89	0.8
^{6}Li—^{12}C	30.6	*S*2	1170.0	9331.0	12.5	0.89	0.8

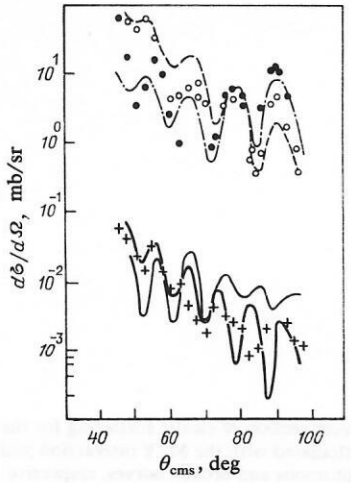

FIG. 21. Cross section of ^{16}O–^{16}O elastic scattering calculated with Skyrme δ-function forces and the corresponding experimental data for $E_{lab} = 41$ MeV (chain curve, open circles), for $E_{lab} = 49$ MeV (broken curve, black circles), and for $E_{lab} = 63$ MeV (broken curve, plus signs).

^4He–^{12}C elastic-scattering cross sections at 139 MeV together with the experimental data of Ref. 53.

For the parameter value $\beta = 0.4$ there is satisfactory agreement with the experimental data up to scattering angles $\theta = 40°$. Thereafter, with increasing scattering angle, the experimental cross section falls off much more rapidly than the theoretical one. One can give numerous reasons for such a discrepancy between theory and experiment. First, as noted above, the Woods–Saxon form is a more realistic one for the absorption potential. Second, the folding potential itself may be corrected by various factors—dependence of the effective interaction on the density of the matter distribution in the nucleus, a contribution of second-order processes, and so forth.

For comparison, Fig. 24 also gives the result of calculation of the cross section with an NN interaction of the type of Skyrme δ-function forces. It can be seen that the difference between the angular distributions for the finite-range forces and the Skyrme δ-function forces is slight. Since the Skyrme interaction includes a density term, but the realistic interaction does not depend on the density of the matter distribution in the nucleus, it is not possible to draw an unambiguous conclusion about the part played by the finite range of the effective forces from these calculations.

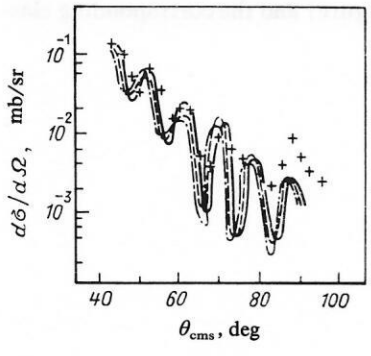

FIG. 22. Experimental data on the cross section of ^{16}O–^{16}O elastic scattering (plus signs) and results of calculation for three variants of Skyrme δ-function forces: a) continuous curve; b) broken curve; c) chain curve from Table II.

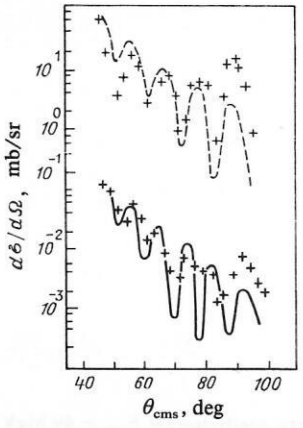

FIG. 23. Cross section of ^{16}O–^{16}O elastic scattering for $E_{lab} = 49$ MeV (broken curve) and $E_{lab} = 43$ MeV (continuous curve) with Satchler–Love Gaussian-type forces (the points are the experimental results).

In Ref. 8, an attempt was made to describe ^{16}O–^{16}O elastic scattering by means of the nuclear interaction potential obtained in the energy-density formalism. The results of the calculation are shown in Fig. 25. This potential has a repulsive core and a relatively small depth. To describe the experimental data, the authors of Ref. 8 were forced to introduce two free parameters: $V = (\alpha + i\beta)U$. For $\alpha = 2.7$ and $\beta = 0.3$, a satisfactory description of the experimental data for $E_{lab} = 49$ MeV could be obtained. However, it was impossible to describe the experiment at $E_{lab} = 63$ MeV in the region of scattering angles $\theta < 80°$.

The investigations of the elastic cross sections made in

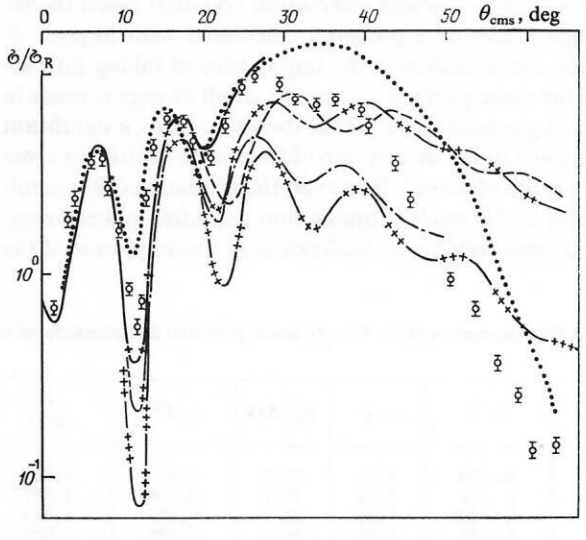

FIG. 24. Results of calculations of the cross sections of ^4He–^{12}C elastic scattering at 139 MeV together with the experimental data of Ref. 53. The dotted curve is for $R = 4.2$, $a = 0.47$, $W_0 = -16.9$; Satchler–Love forces: the curve with single crosses for $\beta = 0.2$, two crosses for $\beta = 0.4$, and three crosses for $\beta = 0.6$; Skyrme δ-function forces: broken curve for $\beta = 0.4$ and chain curve for $\beta = 0.6$.

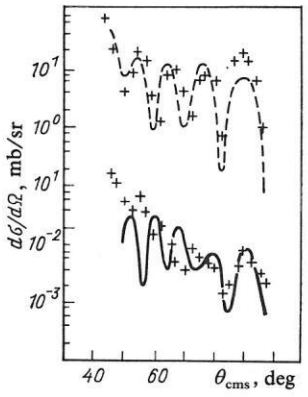

FIG. 25. Cross section of ^{16}O–^{16}O elastic scattering for $E_{lab} = 49$ MeV (broken curve) and $E_{lab} = 63$ MeV (continuous curve) with the potential obtained in the energy-density formalism.

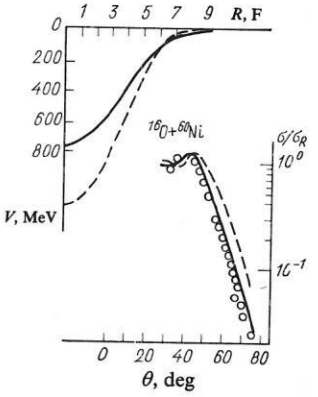

FIG. 26. Folding potential and cross section of elastic scattering for the ^{16}O–^{60}Ni system at 61.42 MeV calculated with the M3Y interaction and with a zero-range interaction: continuous and broken curves, respectively.

Refs. 1 and 6–8 permit a number of general comments to be made.

By means of the microscopic nuclear densities obtained in the method of hyperspherical functions and tested on the experimental data, nuclear interaction potentials for the $A = 4$, 6, 12, 16 ions have been constructed in the folding model and in the energy-density formalism. In this case, by varying just the one parameter of the imaginary part of the optical potential it is possible to obtain a description comparable with the phenomenological description of the differential cross section of elastic scattering of the ions ($A \leqslant 16$), in which it is necessary to use up to six parameters in, for example, the case of the Woods–Saxon potential.

The choice of the *NN* interaction in the determination of the nuclear density determines the behavior of the nuclear interaction potential of the ions at short distances; in the peripheral region, the difference is not important. The more or less equally good description of elastic scattering with either a realistic nuclear interaction potential based on finite-range forces or a potential calculated with Skyrme δ-function forces indicates the importance of taking into account the three-particle forces. If a small change is made in the folding potential in either of these two cases, a significant discrepancy in the description of the elastic-scattering cross section is not observed. However, the appearance of a repulsive core in the nuclear interaction potential makes necessary an appreciable renormalization of the amplitude of the potential. Therefore, the inner part of the nuclear interaction potential can affect the results of the elastic scattering of the ions.

Finally, in Ref. 9 the field of application of the microscopic approach described here was extended and applied to heavier ions. Elastic scattering of the ^{6}Li, ^{12}C, ^{16}O ions by ^{58,60}Ni, ^{90}Zr, ^{124}Sn, ^{142,144}Nd, ^{208}Pb was studied.

In this case, the densities obtained in the method of hyperspherical functions[5] were used for the light ions. The nuclear densities for the heavy ions were found in the framework of the quasiparticle-phonon model.[10] Comparison of these densities with the ones used in the analogous investigations in Refs. 14 and 15 shows that the densities for the light ions from Ref. 5 give a better description of the asymptotic behavior of the nucleus, while the densities for the heavy target ions are actually very close to the shell-calculation densities used in Ref. 14. However, a difference is that the effects of monopole pairing are also taken into account in Ref. 9 for the ground-state densities.

Table IX gives the parameters of the single-particle potential and the pairing constants $G_{N,Z}$ for all the nuclei studied.[13] Figure 26 illustrates the dependence of the results of the calculation of the angular distributions of the heavy-ion elastic-scattering cross sections on the choice of the effective *NN* interaction. Shown here are the folding potentials for the ^{16}O–^{60}Ni system (upper figure) and the corresponding elas-

TABLE IX. Parameters of the Woods-Saxon potential and constants of the pairing interaction.

A	N, Z	r_0, F	V_0, MeV	$\varkappa$, F^2	α, F^{-1}	G_{NZ}, MeV
59	$N=31$	1.31	46.2	0.413	1.613	0.280
	$Z=27$	1.24	53.7	0.378	1.587	0.302
91	$N=53$	1.29	44.7	0.413	1.613	0.168
	$Z=39$	1.24	56.9	0.338	1.587	0.194
121	$N=71$	1.28	43.2	0.413	1.613	0.122
	$Z=51$	1.24	59.9	0.346	1.587	0.136
141	$N=83$	1.27	46.0	0.413	1.613	0.116
	$Z=59$	1.24	57.7	0.349	1.587	0.122
209	$N=127$	1.26	44.8	0.376	1.587	0.074
	$Z=83$	1.24	60.3	0.371	1.587	0.080

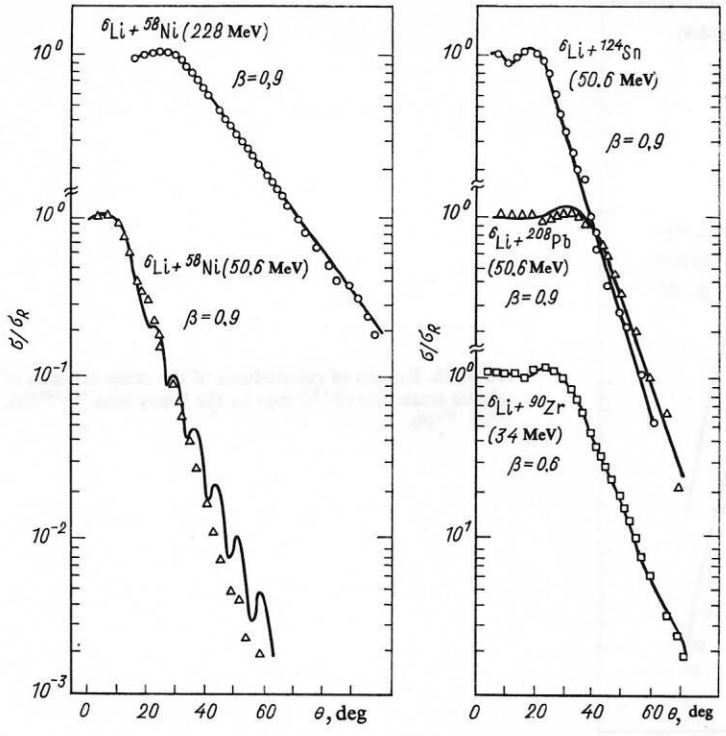

FIG. 27. Results of calculations of the cross sections of elastic scattering of ^{6}Li ions by the heavy ions ^{58,60}Ni, ^{90}Zr, ^{124}Sn, ^{208}Pb.

tic-scattering cross sections at energies [61] and [42] MeV obtained for the two different types of *NN* interaction—the broken curve for the results with Skyrme-type zero-range *NN* forces[29] and the continuous curves for finite-range forces of the Yukawa type M3Y.[14] The points show the experimental data from Ref. 65. The folding potential obtained with the *NN* effective forces M3Y is shallower at short distances between the interacting ions and deeper in the region of the range of strong absorption as compared with the corresponding results for the Skyrme-type δ-function forces. Evidently, the *NN* forces of Yukawa type describe the real situation in the nucleus better. Therefore, the angular distributions obtained with the M3Y forces describe the experimental data better than the corresponding results of the calculation with the δ-function forces. All the subsequent calculations of the elastic-scattering cross sections of heavy ions[9] were made with the M3Y forces. Figure 27 shows the results of calculation of the elastic cross sections of ^{6}Li ions interacting with the heavy ions ^{58}Ni, ^{90}Zr, ^{124}Sn, ^{208}Pb. Here we make a comparison with the experimental cross sections of elastic scattering for ^{6}Li–^{58}Ni at 22.8 MeV from Ref. 66; for the same system at 50.6 MeV from Ref. 67; for the system ^{6}Li–^{90}Zr at 34 MeV from Ref. 68; and, finally, the elastic cross sections for scattering of ^{6}Li ions by the ^{124}Sn and ^{208}Pb nuclei at 50.6 MeV taken from Ref. 67. These investigations show that in the proposed approach, i.e., with nuclear densities obtained in the microscopic method, calculation of the cross sections with just one free parameter makes possible an overall good description of the experimental data.

Figure 27 also shows the results of ^{6}Li–^{58}Ni elastic scattering for two different energies of the incident particles. The calculations showed that it is possible to reproduce the experimental data at different energies with the same amplitude $\beta = 0.9$ of the imaginary part of the optical potential. This conclusion differs from the one obtained in Ref. 6 in the description of ^{6}Li scattering by the light ion ^{12}C. In these calculations, the amplitude of the imaginary part for elastic scattering at 30.6 MeV was four times smaller than the corresponding value at 90 MeV.

Evidently, the amplitude of the imaginary part of the optical potential has less influence on the results of the calculation of the elastic-scattering cross sections for heavy ions than it does for light ions.

Figure 28 gives the results of the calculations in Ref. 9 of the cross sections of elastic scattering of ^{12}C by the nuclei ^{142}Nd and ^{144}Nd at 70.4 MeV, by ^{90}Zr at 98 and 60 MeV, and by ^{208}Pb at 96 MeV, together with the corresponding experimental data from Refs. 69–72. For all the investigated nuclei, except ^{208}Pb, the experimental data on the elastic scattering of the ^{12}C ions can be well described. Further, the amplitude of the imaginary part is appreciably less than in the case of the ^{6}Li ions ($\beta = 0.1$–0.3). This indicates that the density obtained in the method of hyperspherical functions for the ^{12}C nucleus describes the real situation in the nucleus fairly well. An exception is the elastic cross section for scattering of the ^{12}C ion by the ^{208}Pb target. In this case, the description of the elastic-scattering cross section fails from $\theta = 40°$. At the same time, the amplitude of the imaginary part is relatively large, $\beta = 0.7$, in these calculations. It can be seen from Fig. 28 that with the same parameter $\beta = 0.3$ it is possible to describe the cross section of scattering by the isotopes ^{142}Nd and ^{144}Nd at energy 70.4 MeV of the incident particles despite the fact that the ^{142}Nd and ^{144}Nd densities differ in that there is no neutron pairing in the case of the half-magic nucleus ^{142}Nd.

Figure 29 shows the results of the calculation in Ref. 9 of the cross sections of elastic scattering of ^{16}O ions by the ^{60}Ni nucleus at two energies of the incident particles: 61.42

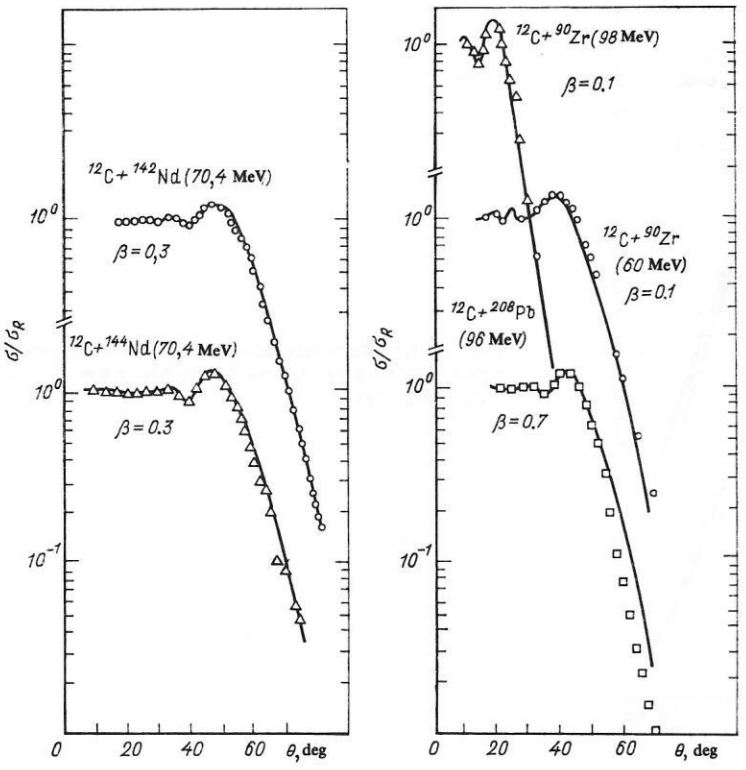

FIG. 28. Results of calculations of the cross sections of elastic scattering of ^{12}C ions by the heavy ions $^{142,144}Nd$, ^{90}Zr, ^{208}Pb.

MeV (Ref. 65) and 141.7 MeV.[73] The results of the calculation showed that the theoretical cross section at the lower energy (61.42 MeV) reproduces the experimental data well, whereas the experimental data on the angular distributions of the ^{16}O–^{60}Ni elastic-scattering cross section at 141.7 MeV cannot be reproduced by any variation of the amplitude in the imaginary part of the optical potential. The most probable reason for this discrepancy is in the inadequate number of partial waves (about 50) taken into account in the calculation of the elastic cross section.

Thus, the theoretical investigation made in Ref. 9 of the cross sections of elastic scattering of the ^{6}Li, ^{12}C, ^{16}O ions by the $^{58,60}Ni$, ^{90}Zr, ^{124}Sn, $^{142,144}Nd$, ^{208}Pb ions showed that overall it is possible to reproduce the experimental results using just one free parameter. The specifically microscopic nature of the wave functions of these nuclei is manifested in these calculations. The amplitude of the imaginary part of the optical potential has less effect for the heavy ions on the results of the calculation of the elastic-scattering cross sections than it does for the light ones.

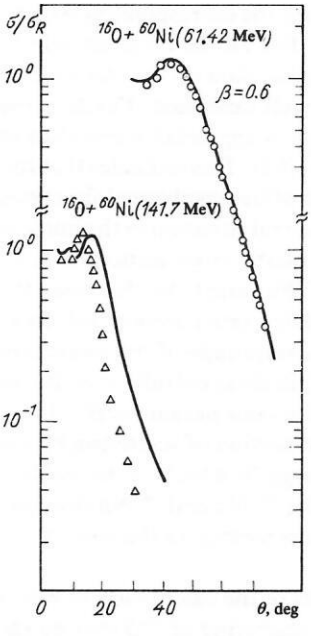

FIG. 29. Results of calculation of the ^{16}O–^{60}Ni elastic cross section.

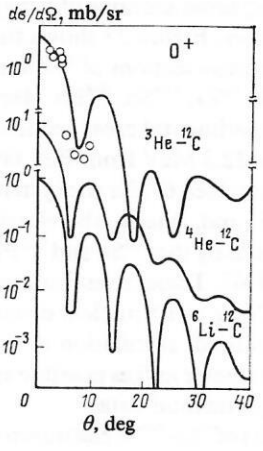

FIG. 30. Results of calculation and comparison of them with experiment (points) for the cross section of inelastic scattering with 0^+ ($E_{ex} = 20.3$ MeV) excitation in the ^{12}C nucleus for different incident particles: ^{3}He, ^{4}He, ^{6}Li.

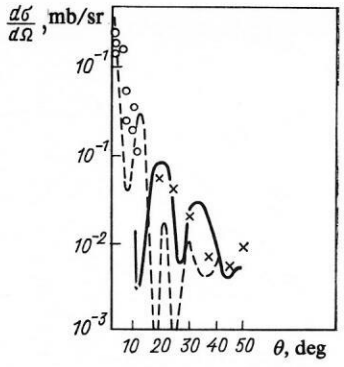

FIG. 31. Comparison of experimental data (points) and results of calculation for the inelastic cross section of scattering with excitation of a monopole resonance in ^{4}He and ^{12}C. The continuous curve is for $E_{ex}^{\alpha} = 20.2$ MeV, the broken curve for $E_{ex}^{^{12}C} = 20.3$ MeV.

Investigation of the cross sections of inelastic scattering of ions with excitation of the giant monopole resonance

The microscopic approach described in this review was used to study the cross sections of inelastic scattering of ions[2] with excitation of the states of the giant monopole resonance in light nuclei.

The angular distribution of the cross section was studied in the coupled-channel method. The amplitude of the imaginary part of the optical potential was taken to be proportional to its real part and was normalized in the elastic channel.

As was noted above, these investigations are topical, since, on the one hand, there have been numerous attempts in recent years to detect and identify giant monopole resonances in nuclei.[74–82] However, the existence of monopole resonances in light nuclei ($A \leqslant 16$) still remains open.

In particular, in Ref. 74 experimental results were obtained on the cross section of inelastic scattering with excitation of a 0^+ state at energy 20.3 MeV and width 1 MeV of the

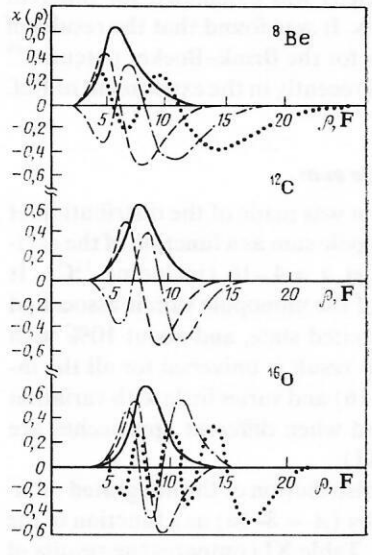

FIG. 32. Radial wave functions $\chi(\rho)$ for the ground and monopole-excited states of the ^{8}Be, ^{12}C, ^{16}O nuclei.

^{12}C nucleus in the ^{3}He–^{12}C reaction, and the nature of this state was discussed.

On the other hand, the method of hyperspherical functions should make reliable theoretical predictions in the description of monopole vibrations.[3] Therefore, a detailed investigation was made in Ref. 2 of inelastic cross sections of reactions with excitation of a monopole resonance in ^{12}C. The computational scheme included the densities for the ground and monopole-excited states of the nuclei as obtained in the method of hyperspherical functions.[5] The results of the calculation are shown in Fig. 30, which gives the inelastic cross sections with the 0^+ ($E_{ex} = 20.3$ MeV) excitation in the ^{12}C nucleus for different incident particles, ^{3}He, ^{4}He, ^{6}Li, and the corresponding experimental data for the ^{3}He–^{12}C system are also shown.

In Ref. 77, the manifestation of giant monopole resonances in elastic scattering of ions by the ^{4}He nucleus was considered. A calculation was made of the cross section of inelastic scattering of the ^{12}C nucleus by a ^{4}He target with excitation of a monopole resonance in the ^{4}He nucleus at energy $E_{ex} = 20.2$ MeV. The results of the calculation and a comparison of them with the experimental data from Ref. 78 are shown in Fig. 31. The results of the calculations in Refs. 2 and 77 are in satisfactory agreement with the description of the experimental data without an additional renormalization of the parameters of the *NN* interaction in either the elastic or the inelastic channel.

Thus, in the microscopic approach described here with just one free parameter it is possible to reproduce the elastic and inelastic cross sections of reactions with heavy ions with a degree of accuracy only slightly less than that achieved with the phenomenological Woods–Saxon potential containing six free parameters. However, in the microscopic approach the reduced probabilities of monopole transitions are calculated using the wave functions of the ground state and 87 obtained by means of other models.

Width of giant monopole resonance

In the method of hyperspherical functions it becomes obvious that among the giant resonances of different multipolarities the giant monopole resonances are distinguished by their small width. This is determined by the specific nature of their radial wave function. In Fig. 34 (Ref. 83) we show as examples the effective potentials and solutions in them for the ^{16}O nucleus corresponding to the monopole and dipole resonances, and also the effective potential and the solutions in it for the ground state of the neighboring nucleus (^{15}O). It can be seen that both the spreading width and the decay width of the monopole resonance, to which the wave function with a node corresponds, must be appreciably less than the corresponding widths of the resonances of other multipolarities, which have radial wave functions without a node. Indeed, these widths are determined by the integrals of overlap of the intrinsic wave function with either the wave functions of other multipolarities or the ground-state wave function of the final nucleus. As an example, estimates were made in Ref. 83 of the decay widths of the giant monopole resonance of the ^{16}O nucleus with emission of α particles,

TABLE X. Binding energy, excitation energy of giant monopole resonances, rms radii, and the distribution of the monopole sum (16) of light nuclei.

Nucleus	N	E_{bd}, MeV	E_{ex}, MeV	$\langle r^2\rangle_{ii}^{1/2}$, F	S_{0i}, %
^{4}He	0	−28,00	0	1,767	0
	1	−3,68	24,32	3,487	74,7
^{8}Be	0	−40,12	—	2,353	—
	1	−21,59	18,63	2,940	90,4
	2	−9,23	30,89	3,774	6,5
	3	−1,99	38,03	5,116	1,2
^{12}C	0	−83,40	—	2,385	—
	1	−61,57	21,53	2,689	95,6
	2	−43,78	39,32	3,046	3,5
	3	−29,43	53,67	3,474	0,4
	4	−18,21	64,99	4,000	0,1
	5	−9,79	73,31	4,671	0,0
	6	−3,84	79,26	5,572	—
^{16}O	0	−146,52	0	2,252	—
	1	−121,14	25,38	2,449	90,6
	2	−98,74	47,78	2,665	2,2
	3	−79,14	67,38	2,904	0,2
	4	−62,06	84,46	3,173	0,0
	5	−47,70	99,12	3,476	—
	6	−34,98	112,54	3,823	—
	7	−24,64	122,88	—	—

the excited state of the nucleus, whereas in the phenomenological approach they are extracted from analysis of the inelastic cross section.

The results of the estimate of the monopole sum rule obtained in Ref. 74 in a phenomenological description of the inelastic scattering of 108.5-MeV ^{3}He particles on the ^{12}C nucleus at small angles do not agree with the results of Ref. 2, in which a microscopic calculation was made using nuclear densities obtained in the framework of the method of hyperspherical functions. In this connection, we consider briefly below some results obtained in the method of hyperspherical functions in the description of the properties of giant monopole resonances of light nuclei. In Refs. 2–4 and 83, investigations were made in the formalism of hyperspherical functions, and these predicted the properties of the monopole resonances in the light nuclei. The excitation energies, width, and monopole sum rule were studied. Figure 32 shows the radial wave functions $\chi(\rho)$ for the ground and monopole-excited states of the ^{8}Be, ^{12}C, ^{16}O nuclei; Table X gives the excitation energies of the giant monopole resonances, the mean-square radii, and the distribution of the monopole sum of the light nuclei from Ref. 4. Overall, the results of the theoretical predictions of Ref. 4 were confirmed in the experiment,[74] but there are differences in the estimate of the monopole sum rule. We analyze this question in more detail for the example of the ^{12}C nucleus, since it was for this nucleus that in Ref. 74 a high-lying monopole level at excitation energy $E_{ex} = 20.3$ MeV was discovered.

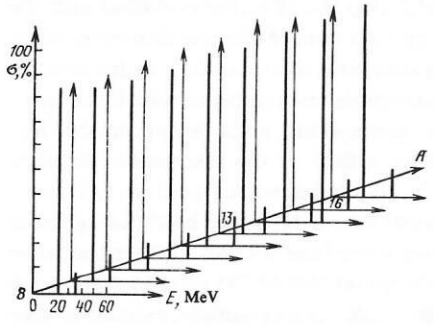

FIG. 33. Distribution of the integrated monopole sum of light nuclei (A = 8–16) as a function of the excitation energy.

Excitation energy of the giant monopole resonance of the ^{12}C nucleus

In Ref. 5, the excitation energy of the giant monopole resonance of the ^{12}C nucleus was calculated for different nucleon-nucleon potentials. It was found that the results of the theoretical predictions for the Brink–Boeker potential[39] agree with the value found recently in the experiment of Ref. 74.

Energy-weighted monopole sum

In Ref. 4, a calculation was made of the distribution of the energy-weighted monopole sum as a function of the excitation energy for the nuclei $A = 4-16$ (including ^{12}C). It was shown that 70–90% of the monopole sum is associated with the first monopole-excited state, and about 10% with the second. Moreover, this result is universal for all the investigated nuclei ($A = 4-16$) and varies little with variation of the NN interactions and when different approaches are used (Fig. 33 and Table XI).

Figure 33 shows the distribution of the integrated monopole sum of the light nuclei (A = 8–16) as a function of the nuclear excitation energy. Table XI compares the results of calculation of the properties of the giant monopole resonance of the ^{16}O nucleus made by the method of hyperspher-

TABLE XI. Results of calculation of the distribution of the integrated monopole sum of the nucleus ^{16}O in various models.

Reference	ΔE, MeV	σ, %	Reference	ΔE, MeV	σ, %
[3]	29 52	59 11	[85]	24	56
[84]	27 50 70	68 6 1	[86]	15—30 29—35 35—50	51 31 11
			[87]	30,5	—

ical functions for the Volkov potential[40] and for a Yukawa-type potential[84] with the corresponding results of Refs. 85–protons, and neutrons. The value obtained for this width was about 1 MeV. These predictions are also in agreement with the experimental results of Ref. 74.

Thus, the investigation made in the framework of the method of hyperspherical functions indicates a collective nature of the high-lying excited 0^+ ($E_{ex} = 20.3$ MeV) state in the ^{12}C nucleus.

The microscopic approach proposed here can also be applied to the study of inelastic cross sections of reactions with heavy ions when states of other multipolarity are excited.

CONCLUSIONS

In the review, we have presented a microscopic approach to the study of elastic and inelastic cross sections of reactions with heavy ions.

To construct the interaction potential of two heavy particles this uses nuclear densities obtained in microscopic models and tested on a set of experimental data. For light nuclei, the densities were calculated in the method of hyperspherical functions; for heavy ions, in the framework of the quasiparticle-phonon model.

In such an approach, not only the interaction potentials in the ground state but also the corresponding potentials in an excited state have been obtained, together with the non-diagonal matrix elements of the potential describing inelastic processes.

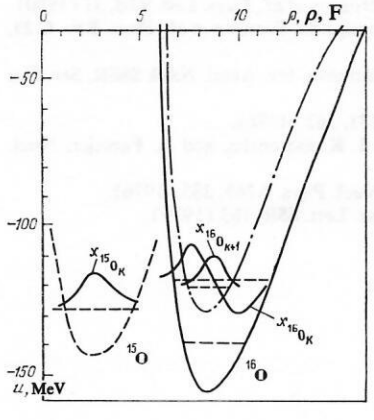

FIG. 34. Effective potentials and solutions in them for different states of the nuclei ^{15}O and ^{16}O. The continuous curve gives the results of the calculation for the ^{16}O nucleus in the ground state, the broken curve gives the corresponding data for the ^{15}O nucleus in the ground state, and the chain curve gives the results of the calculation for the ^{16}O nucleus in the state J^π, $T = 1^-$, 1.

Scattering cross sections of heavy ions have been calculated with one free parameter, only the amplitude of the forces in the imaginary part of the optical potential being varied.

The calculations showed that the method is universal for the description of the elastic and inelastic cross sections of reactions with heavy ions. Good agreement with the experimental data could be obtained without additional renormalization of the parameters of the calculations in the elastic and inelastic channels.

Thus, in the microscopic approach presented here it is possible to reproduce the elastic and inelastic cross sections of reactions with heavy ions using a single free parameter and with a degree of accuracy only slightly less good than when the phenomenological Woods–Saxon potential containing six free parameters is used. However, in the microscopic approach the reduced transition probability is calculated using the wave functions of the ground and the excited state of the nucleus, whereas in the phenomenological approach these quantities are extracted from an analysis of the inelastic reaction cross section. Therefore, the knowledge of the nature of the wave function that is used in the calculations opens up possibilities for studying nuclear structure in reactions with heavy ions. In such a formalism, we have considered the possible manifestation of giant monopole resonances in light nuclei. Predictions for the excitation energy, the energy-weighted monopole sum, and the widths of such resonances have been made. Some of these predictions have been confirmed by the experiments at Grenoble.

The proposed method can also be used to study inelastic cross sections of reactions with heavy ions when states of other multipolarity are excited.

It is a pleasant duty to express my thanks to V. G. Solov'ev, F. Gareev, and V. M. Shilov, the numerous discussions with whom greatly assisted in the writing of the present review, and also V. V. Burov, R. Dymarz, M. Kaschiev, Dao Tien Khoa, R. G. Nazmitdinov, G. Saupe, and A. A. Shirokova, with whom some of the results included in this review were obtained in collaboration.

[1]R. Dymarz, J. L. Molina, and K. V. Shitikova, Z. Phys. A **299**, 245 (1981).
[2]R. Dymarz and K. V. Shitikova, Preprint E7-81-653 [in English], JINR, Dubna (1981).
[3]K. V. Shitikova, Nucl. Phys. A **231**, 365 (1979).

[4]M. Kaschiev and K. V. Shitikova, Yad. Fiz. **30**, 1479 (1979) [Sov. J. Nucl. Phys. **30**, 766 (1979)].
[5]V. V. Burov, V. N. Dostovalov, M. Kaschiev, and K. V. Shitikova, J. Phys. G **7**, 139 (1981).
[6]A. S. Dem'yanova and K. V. Shitikova, Yad. Fiz. **35**, 1431 (1982) [Sov. J. Nucl. Phys. **35**, 835 (1982)].
[7]V. V. Burov, O. M. Knyazkov, A. A. Shirokova, and K. V. Shitikova, Z. Phys. A **313**, 319 (1983).
[8]R. G. Nazmitdinov, G. Saupe, and K. V. Shitikova, Preprint E4-83-368 [in English], JINR, Dubna (1983); Yad. Fiz. **39**, 1415 (1984) [Sov. J. Nucl. Phys. **39**, 894 (1984)].
[9]Dao Tien Khoa and K. V. Shitikova, Preprint E4-84-305 [in English], JINR, Dubna (1984).
[10]V. G. Solov'ev, Fiz. Elem. Chastits At. Yadra **9**, 580 (1978) [Sov. J. Part. Nucl. **9**, 226 (1978)].
[11]Yu. A. Simonov, Yad. Fiz. **3**, 630 (1966) [Sov. J. Nucl. Phys. **3**, 461 (1966)]; A. I. Baz' *et al.*, Fiz. Elem. Chastits At. Yadra **3**, 3 (1972) [Sov. J. Part. Nucl. **3**, 1 (1972)]; Yu. F. Smirnov and K. V. Shitikova, Fiz. Elem. Chastits At. Yadra **8**, 847 (1977) [Sov. J. Part. Nucl. **8**, 344 (1977)].
[12]A. N. Vdovin and V. G. Solov'ev, Fiz. Elem. Chastits At. Yadra **14**, 237 (1983) [Sov. J. Part. Nucl. **14**, 99 (1983)].
[13]V. Yu. Ponomarev *et al.*, Nucl. Phys. **A323**, 446 (1979).
[14]G. R. Satchler and W. G. Love, Phys. Lett. **65B**, 415 (1976); Phys. Rep. **55**, 183 (1979).
[15]G. R. Satchler, *Direct Nuclear Reactions,* Oxford University Press, New York (1983).
[16]H. Feshbach, Ann. Phys. (N.Y.) **19**, 287 (1962).
[17]R. J. Lombard, Ann. Phys. (N.Y.) **77**, 380 (1973); H. Ngo and Ch. Ngo, Nucl. Phys. **A388**, 140 (1980).
[18]G. W. Greenless, G. J. Pyle, and Y. C. Tang, Phys. Rev. **171**, 1115 (1968).
[19]B. C. Sinha, Phys. Rep. **20**, 1 (1975).
[20]F. Izumoto, S. Krewald, and A. Faessler, Nucl. Phys. **A357**, 471 (1981).
[21]S. B. Khadkikar, L. Rikus, and A. Faessler, Nucl. Phys. **A369**, 495 (1981).
[22]R. Sartor and A. Faessler, Nucl. Phys. **A376**, 263 (1982).
[23]A. Faessler, L. Rikus, and S. B. Khadkikar, Nucl. Phys. **A401**, 157 (1983).
[24]G. Rana, C. Ngô, A. Faessler *et al.*, Nucl. Phys. **A414**, 309 (1984).
[25]G. Spitz, K. Hahn, and E. W. Schmid, Z. Phys. A **303**, 209 (1981).
[26]K. L. Kowalski and A. Picklesimer, Nucl. Phys. **A369**, 336 (1981).
[27]K. S. Panda, B. Behera, and R. K. Satpathy, J. Phys. G **7**, 937 (1981).
[28]F. J. Vinas, M. Lorano, and G. Maturga, Phys. Rev. C **23**, 780 (1981).
[29]T. H. R. Skyrme, Philos. Mag. **1**, 1043 (1958); D. Vautherin and D. M. Brink, Phys. Lett. **32B**, 149 (1970).
[30]F. Toudeur, M. Brack, M. Farine, and J. M. Pearson, Nucl. Phys. **A420**, 297 (1984).
[31]O. M. Knyaz'kov, Vestn. Mosk. Univ. Fiz. Khim. **10**, 34 (1980).
[32]O. M. Knyaz'kov, Yad. Fiz. **33**, 1176 (1981) [Sov. J. Nucl. Phys. **33**, 624 (1981)].
[33]O. M. Knyaskov and E. F. Hefter, Z. Phys. **A301**, 277 (1981).
[34]N. Bogdanova, A. A. Shirokova, and K. V. Shitikova, Preprint R4-83-547 [in Russian], JINR, Dubna (1983).
[35]N. Vinh-Mau, Phys. Lett. **71B**, 5 (1977).
[36]Y. Goto and M. Horinchi, Prog. Theor. Phys. **62**, 662 (1979).
[37]M. Kamimura, Nucl. Phys. **A351**, 273 (1981).
[38]V. K. Luk'yanov and Yu. S. Pol', Fiz. Elem. Chastits At. Yadra **5**, 955 (1974) [Sov. J. Part. Nucl. **5**, 385 (1975)].
[39]D. M. Brink and E. Boeker, Nucl. Phys. **A91**, 1 (1967).
[40]A. B. Volkov, Nucl. Phys. **A74**, 33 (1965).
[41]V. V. Burov and V. K. Luk'yanov, Preprint R4-11098 [in Russian], JINR, Dubna (1977).
[42]C. Weruttz and H. Uberall, Phys. Rev. **149**, 762 (1966); M. Baumgartner, H. P. Gubler, M. Heller *et al.*, Nucl. Phys. **A368**, 189 (1981).
[43]M. Sontona and J. Zofka, Phys. Rev. C **10**, 2646 (1974).
[44]M. Bouten and M. C. Bouten, Phys. Lett. **26B**, 191 (1968).
[45]M. Bouten and M. C. Bouten, Lett. Nuovo Cimento **22**, 415 (1978).
[46]V. F. Rybachenko, A. A. Sadovoĭ, and N. M. Chulkov, Yad. Fiz. **10**, 1165 (1969) [Sov. J. Nucl. Phys. **10**, 663 (1970)].
[47]G. P. Kamuntavichus, Yad. Fiz. **27**, 98 (1978) [Sov. J. Nucl. Phys. **27**, 52 (1978)].
[48]I. K. Aver'yanov, A. A. Sadovoĭ, N. M. Chulkov, and L. A. Vakhlamova, Yad. Fiz. **17**, 258 (1973) [Sov. J. Nucl. Phys. **17**, 132 (1973)].
[49]R. Dymarz, J. L. Molina, and K. V. Shitikova, in: *Mezhdunarodnyĭ simpozium po sintezu i svoĭstvam novykh élementov* (*Intern. Symposium on the Synthesis and Properties of New Elements*), Dubna (1980), p. 68.
[50]J. L. Molina and K. V. Shitikova, Preprint R7-80-60 [in Russian], JINR, Dubna (1980).
[51]G. Eckart and G. Holzwarth, Z. Phys. A **281**, 385 (1977).
[52]B. Sinha and S. A. Moszkovski, Phys. Lett. **81B**, 288 (1979).
[53]S. M. Smith *et al.*, Nucl. Phys. **A207**, 273 (1973).
[54]P. Schwadt, W. W. Jacobs, M. D. Kaitchuck, *et al.*, Phys. Rev. C **24**, 1522 (1981).
[55]J. Cook, Nucl. Phys. **A375**, 238 (1982).
[56]J. Cook, H. J. Gils, H. Rebel *et al.*, Nucl. Phys. **A388**, 173 (1982).
[57]A. S. Dem'yanova and V. I. Man'ko, Yad. Fiz. **38**, 1189 (1983) [Sov. J. Nucl. Phys. **38**, 716 (1983)].
[58]Z. Majka, H. J. Gils, and H. Rebel, Phys. Rev. C **25**, 2996 (1982).
[59]D. Baye and N. Pecher, Nucl. Phys. **A379**, 330 (1982).
[60]C. L. Woods, B. A. Broun, and N. A. Jelley, J. Phys. G **8**, 1699 (1982).
[61]L. J. B. Goldfarb and Y. K. Gambhir, Nucl. Phys. **A401**, 557 (1983).
[62]A. S. Damyanova and V. I. Manko, in: *Intern. Conf. on Extreme States in Nuclear Systems,* Dresden (1980), p. 46.
[63]D. M. Brink and G. R. Satchler, J. Phys. G **7**, 43 (1981).
[64]J. V. Maher *et al.*, Phys. Rev. **188**, 1665 (1969).
[65]K. E. Rehm *et al.*, Phys. Rev. C **12**, 1945 (1975).
[66]W. Weiss *et al.*, Phys. Lett. **61B**, 237 (1976).
[67]L. T. Chua *et al.*, Nucl. Phys. **A273**, 243 (1976).
[68]R. J. Puigh and K. W. Kemper, Nucl. Phys. **A313**, 363 (1979).
[69]D. L. Hills *et al.*, Phys. Rev. C **16**, 1467 (1977).
[70]S. T. Thornton *et al.*, Phys. Rev. C **13**, 1502 (1976).
[71]T. R. Renner, Phys. Rev. C **19**, 765 (1979).
[72]J. B. Ball *et al.*, Nucl. Phys. **A252**, 208 (1975).
[73]G. R. Satchler *et al.*, Nucl. Phys. **A298**, 313 (1978).
[74]D. Lebrun, M. Buenard, P. Martin *et al.*, Phys. Lett. **97B**, 358 (1980).
[75]M. Buenard, D. Lebrun, P. Martin *et al.*, Phys. Rev. Lett. **45**, 1667 (1980).
[76]U. Garg, P. Bogucki, J. D. Bronson *et al.*, Phys. Rev. Lett. **45**, 1670 (1980).
[77]R. G. Nazmitdinov, G. Saupe, A. A. Shirokova, and K. V. Shitikova, in: *Proc. of the Intern. Conf. on Nuclear Physics,* Vol. 1, Florence (1983), p. 492.
[78]R. Jahn *et al.*, Phys. Lett. **65B**, 339 (1976).
[79]D. H. Youngblood, P. Boguchi, J. D. Bronson *et al.*, Phys. Rev. C **23**, 1997 (1981).
[80]H. P. Morsch, M. Bogge, T. Turek *et al.*, Phys. Rev. C **20**, 1600 (1979).
[81]Y. W. Lui, P. Bogucki, J. D. Bronson *et al.*, Phys. Lett. **93B**, 31 (1980).
[82]C. M. Rozsa, D. H. Youngblood, J. D. Bronson *et al.*, Phys. Rev. C **21**, 1252 (1980).
[83]A. A. Shirokova and K. V. Shitikova, Izv. Akad. Nauk SSSR, Ser. Fiz. **43**, 2396 (1979).
[84]G. L. Strobel, Nucl. Phys. **A271**, 162 (1976).
[85]S. Krewald, R. Rosenfelder, I. K. Galonska, and A. Faessler, Nucl. Phys. **A269**, 112 (1976).
[86]K. F. Liu and G. E. Brown, Nucl. Phys. **A265**, 385 (1976).
[87]J. Blocki and H. Flooard, Phys. Lett. **85B**, 163 (1979).

Translated by Julian B. Barbour